ACS ORGANIC & INORGANIC Au
AN OPEN ACCESS JOURNAL OF THE AMERICAN CHEMICAL SOCIETY

pubs.acs.org/orginorgau
Perspective

Anionic Redox Topochemistry for Materials Design: Chalcogenides and Beyond

Published as part of ACS Organic & Inorganic Au virtual special issue "2023 Rising Stars in Organic and Inorganic Chemistry".

Shunsuke Sasaki,* Simon J. Clarke, Stéphane Jobic, and Laurent Cario

Cite This: ACS Org. Inorg. Au 2024, 4, 26−40
Read Online

ABSTRACT: Topochemistry refers to a generic category of solid-state reactions in which precursors and products display strong filiation in their crystal structures. Various low-dimensional materials are subject to this stepwise structure transformation by accommodating guest atoms or molecules in between their 2D slabs or 1D chains loosely bound by van der Waals (vdW) interactions. Those processes are driven by redox reactions between guests and the host framework, where transition metal cations have been widely exploited as the redox center. Topochemistry coupled with this cationic redox not only enables technological applications such as Li-ion secondary batteries but also serves as a powerful tool for structural or electronic fine-tuning of layered transition metal compounds. Over recent years, we have been pursuing materials design beyond this cationic redox topochemistry that was mostly limited to 2D or 1D vdW systems. For this, we proposed new topochemical reactions of non-vdW compounds built of 2D arrays of anionic chalcogen dimers alternating with redox-inert host cationic layers. These chalcogen dimers were found to undergo redox reaction with external metal elements, triggering either (1) insertion of these metals to construct 2D metal chalcogenides or (2) deintercalation of the constituent chalcogen anions. As a whole, this topochemistry works like a "zipper", where reductive cleavage of anionic chalcogen−chalcogen bonds opens up spaces in non-vdW materials, allowing the formation of novel layered structures. This Perspective briefly summarizes seminal examples of unique structure transformations achieved by anionic redox topochemistry as well as challenges on their syntheses and characterizations.

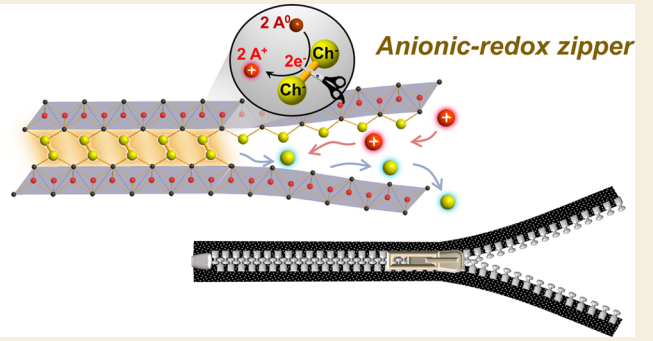

KEYWORDS: *Topochemistry, Anionic redox, Intercalation, Chalcogenides, Low-dimensional materials*

INTRODUCTION

Functionalities of materials are inherently linked to their underlying structures. As such, chemists aspire to achieve the precise manipulation of constituent atoms and their arrangements. Numerous enzymes in biological systems adeptly cleave or connect targeted chemical bonds, a feat similarly achieved through modern genome-editing technology[1] and coupling reactions in organic chemistry.[2] These advancements have enabled tailored designs of intricate molecular structures endowed with the desired functionalities. A similar question then arises concerning inorganic solid-state materials: can a comparable capacity for chemical bond editing be attained for minerals, ceramics, and metals without destroying their overall crystal structures?

In fact, stepwise structure transformations have been widely examined in extended nonmolecular solids. Already in the 1930s, pioneering studies from Hofmann and several other mineralogists have revealed that layered compounds such as graphite[3,4] and clay minerals[4,5] could take up guest species between their rigid 2D slabs. These early investigations were followed by discoveries of many layered transition metal compounds that can host alkali metal cations and organic molecules; some of the seminal examples range from chalcogenides (e.g., MCh_2; M = Group IV−VI elements, Ch = S, Se)[6,7] to oxides (e.g., V_2O_5 and MoO_3),[8,9] halides (e.g., PbI_2 and BiI_3),[10] oxyhalides (e.g., FeOCl),[11] and phosphorus trichalcogenides $MPCh_3$ (M = Fe, Ni, Mn, Ch = S, Se).[12] Since

Received: August 30, 2023
Revised: October 16, 2023
Accepted: October 17, 2023
Published: November 7, 2023

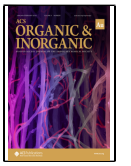

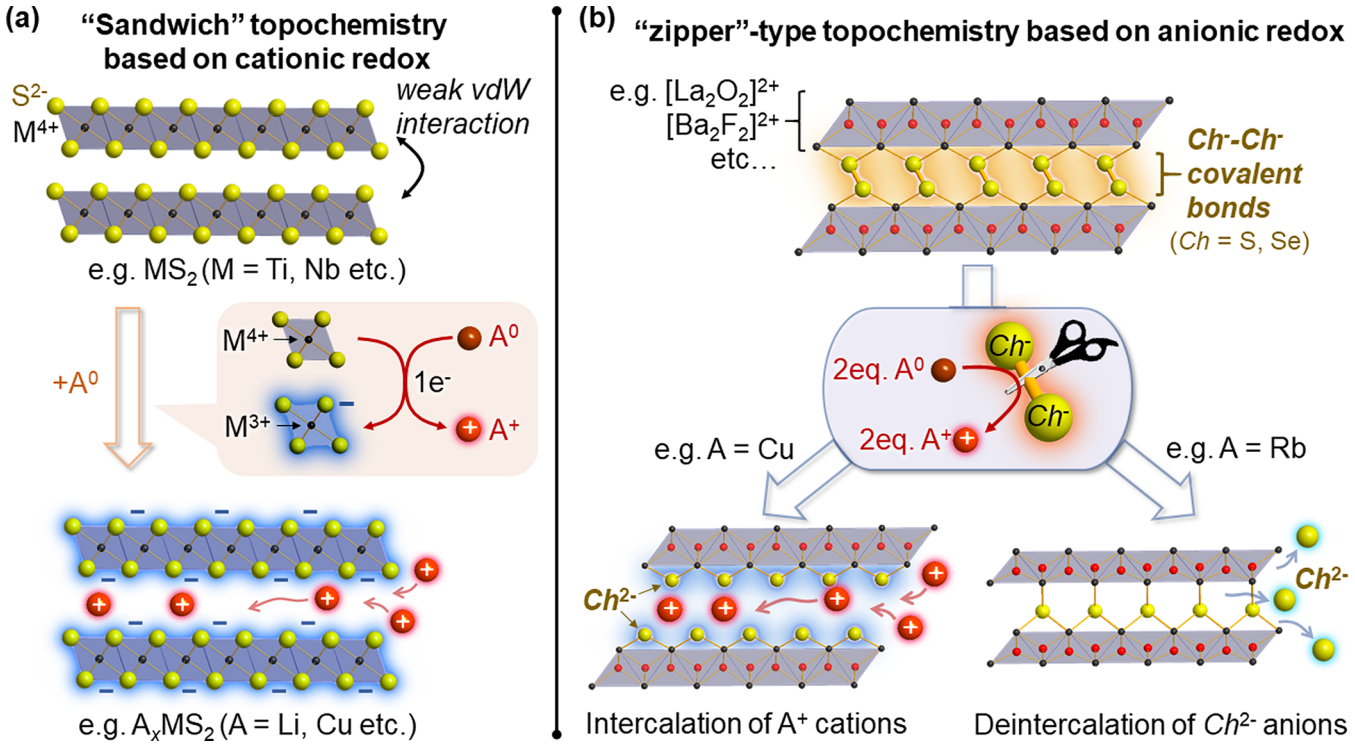

Figure 1. Comparison between (a) conventional topochemistry such as intercalation into 2D van der Waals (vdW) compounds MS_2, and (b) topochemistry that cleaves chalcogen−chalcogen covalent bonds interconnecting the redox-inert, 2D cationic slabs.

2D sheets comprising those host frameworks are bound together only by weak van der Waals (vdW) interactions, intercalation of guest species proceeds under mild conditions, enabling design of metastable sandwichlike compounds inaccessible via conventional high-temperature syntheses (Figure 1a).

Furthermore, these intercalation processes are coupled with a redox reaction between guest species and transition metal cations embedded in the host framework. Taking TiS_2 as an example, intercalation of elements which form monovalent cations A^+ accompanied reduction of host Ti^{4+} cations to Ti^{3+} to balance out overall charge neutrality, which was indeed the basis of the first prototypical Li-ion secondary battery conceived by Whittingham and co-workers.[13] Besides such technological applications, this cationic redox made intercalation processes useful in materials design, particularly for controlling the electronic band filling of low-dimensional compounds. To cite recent remarkable examples, electron doping by intercalation of cationic species induced unconventional superconductivity with e.g. topologically nontrivial states in $Cu_xBi_2Se_3$ ($x \sim 0.3-0.5$)[14] or with Ising spin−orbit coupling in intercalated bulk $NbSe_2$.[15] In the reverse process, deintercalation of K^+ cations converted semiconducting $K_xFe_{1-y}S_2$ ($x \sim 0.8$, $y \sim 0.4$) into the superconducting 2D FeS,[16,17] and this was later applied to prepare 2D itinerant ferromagnet CoCh (Ch = S, Se) from KCo_2Ch_2.[18]

Intercalations and deintercalations mentioned above can be regarded as a simple host−guest chemistry that inserts or removes chemical species in/from between preformed 2D slabs. Meanwhile, there are increasing numbers of reports that demonstrate drastic structure transformations, yet in stepwise and controlled manner. One highlight example is the use of hydride reagents to remove the apical O^{2-} anions from $LaNiO_3$ perovskite, converting this 3D compound into 2D infinite-layer $LaNiO_2$ with Ni^+ under square-planar coordination.[19] Similar reactions were applied to design 2D $SrFeO_2$[20] and more recently superconducting nickelate $Nd_{0.8}Sr_{0.2}NiO_2$[21] as well as the related $CaCoO_2$ phase.[22]

Such removal of bulky O^{2-} anions transforms the topology of transition metal oxide lattices from 3D to 2D, making accessible unexplored chemical spaces of infinite-layer systems. This exemplifies that the scope of materials that one can conceive will be greatly extended by developing novel types of structure transformation. Such importance of reaction design is well recognized in organic synthetic chemistry, which has been devoting incessant efforts to cut and connect specifically targeted moieties of molecules, including relatively strong C−C[23] and C−H bonds.[24] In inorganic solid-state chemistry, stepwise and controlled structure transformations, herein referred to using a generic term "topochemistry",[25] have just started to go beyond conventional intercalation chemistry shown in Figure 1a, and its advance will be one of the next major challenges in this field.

To further evolve topochemistry and extend its scope, we have recently proposed to exploit redox activity of covalent anion−anion bonds.[26] The overall scheme of the concept is depicted in Figure 1b; this novel topochemistry no longer requires the host framework to be a 2D or 1D vdW system with transition metal cations but instead uses non-vdW compounds built of 2D arrays of anionic chalcogen dimers $[Ch_2]^{2-}$ (Ch = S, Se, Te) interconnecting redox-inert, host cationic slabs. Instead of cationic redox, their anionic $[Ch_2]^{2-}$ dimers were found to undergo redox reactions with external zerovalent metals, leading to reductive Ch−Ch bond cleavage: $[Ch_2]^{2-} + 2\ A^0 \rightarrow 2\ Ch^{2-} + 2\ A^+$. This anionic redox opened up spaces to accommodate the guest A^+ cations by unfastening covalent Ch−Ch bonds that join the redox-inert 2D slabs. As a whole, this metal intercalation enabled construction of 2D

https://doi.org/10.1021/acsorginorgau.3c00043
ACS Org. Inorg. Au 2024, 4, 26−40

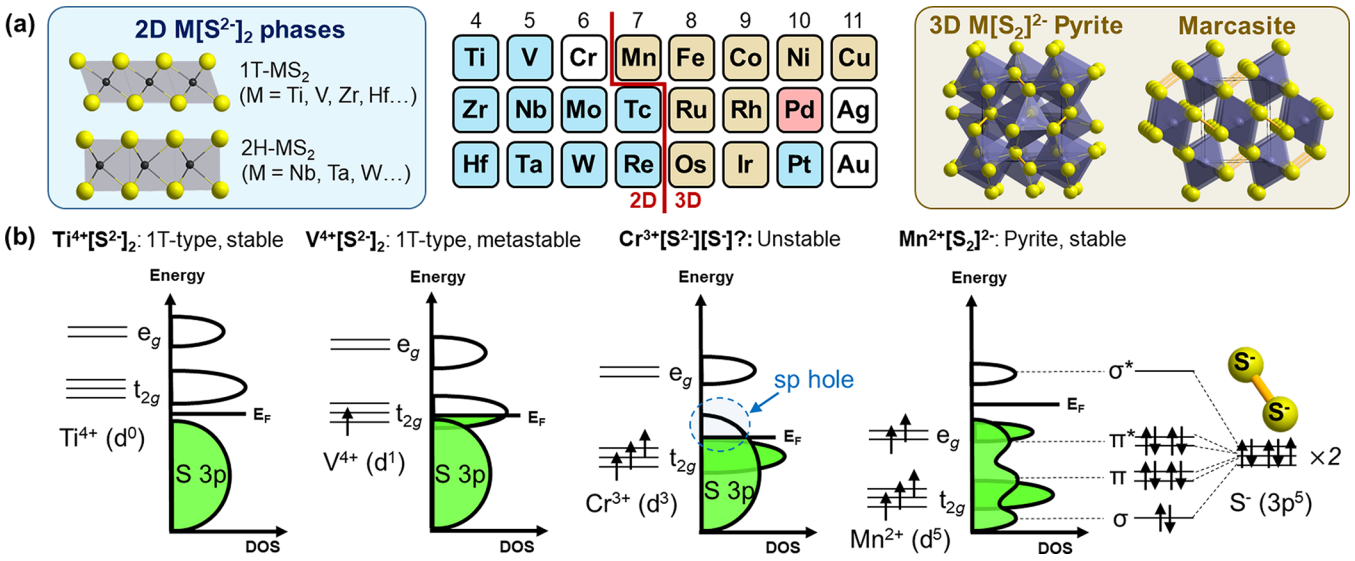

Figure 2. Competition between cationic and anionic redox in transition metal disulfides MS_2. (a) 2D and 3D structures found among the MS_2 binary phases. In the periodic table, transition metal elements taking 2D structures are marked in blue while those displaying 3D structures with S−S bonds are marked in brown. PdS_2, marked in red, shows 2D structure but with S−S bonds.[33] See refs 34 and 35 for more details including the cases of other chalcogen elements. (b) Schematic diagram describing relative positions of transition metal d bands (O_h field) and S 3sp bands for M = Ti, V, Cr, and Mn cases. Note that the diagram reflects neither on-site repulsion nor covalency of d-bands in order to represent redox competition in the simplest way. See refs 34 and 36 for the schemes closer to the real band structure.

metal chalcogenides $[A_2Ch_2]^{2-}$ between host cationic slabs such as $[La_2O_2]^{2+}$ and $[Ba_2F_2]^{2+}$ layers. While an analogy was often made between conventional intercalation compounds and sandwiches or millefeuilles, this novel topochemistry rather resembles the process that opens or closes a zipper of non-vdW compounds. To highlight the uniqueness of this structure transformation benefiting from anionic redox, we herein call it "zipper"-type topochemistry, taking inspiration from the recent analogy used by Bhaskar et al.[27]

Another way to balance the surplus negative charge imposed by reductive Ch−Ch bond cleavage is to remove part of the anionic constituents. In fact, we discovered that the "zipper"-type anionic redox could also lead to deintercalation of Ch^{2-} anions[28] (See Figure 1b). Taking $La_2O_2S_2$ for example, the reaction can be formulated as $[La_2O_2]^{2+}[S_2]^{2-} + 2\ A^0 \rightarrow [La_2O_2]^{2+}[S]^{2-} + A_2S$. This reductive transfer of anionic species resembles electrochemical "conversion" processes well-known for oxides (e.g., $CoO + 2Li^+ + 2e^- \rightarrow Co^0 + Li_2O$)[29] and chalcogenides (e.g., $FeS_2 + 4Li^+ + 4e^- \rightarrow Fe^0 + 2Li_2S$ through Fe−S and/or Li−Fe−S intermediate phases).[30−32] However, the case in Figure 1b is distinct from those conversion processes since it proceeds in a topochemical manner, i.e., without destroying other structural motifs, and that feature will allow controlled design of new metastable structures.

This short review briefly summarizes several preliminary examples that utilized anionic redox topochemistry for the design of new solid-state materials through unique structure transformations. Then its challenges and perspectives are addressed from a methodological point of view, with the hope of inspiring future advancement in this infant but flourishing field.

ANION−CATION REDOX COMPETITION AND TOPOCHEMISTRY

Before describing the actual examples highlighting how anion redox can be useful to alter crystal structures, we herein start from a brief discussion about how anionic species take part in redox processes of topochemistry. We note also that in contrast to its scarcity in materials design, the redox activity of anionic species has been a long-standing subject in electrochemistry.

As described above, it was primarily cationic redox that was used in conventional intercalation chemistry. An archetypical example is the 2D MS_2 phases with the expected $M^{4+}[S^{2-}]_2$ charge balance (Figure 2a). They adopt different coordination geometries (e.g., octahedral in 1T, trigonal prism in 2H, or both)[35] depending on the electron count of the transition metal center M, but have in common the presence of a 2D vdW gap and fully reduced S^{2-} anions. Since the transition metal d bands lie well above the filled sulfur 3p bands (Figure 2b), electrons are readily filled or depleted into/from these cationic d bands during intercalation.

On traversing the periodic table from left to right, the transition metal d levels get gradually lowered. In the case of M = V, the 3d t_{2g} levels approach the top of the S^{2-} 3p band, hindering depletion of their d-electrons.[36] VS_2 with the formal d^1 configuration and the layered structure cannot be synthesized by reacting elemental vanadium and sulfur at high temperature ($V_{1+x}S_2$ and V_5S_8 form instead).[37] In fact, this metastable compound must be prepared from $LiVS_2$ through soft-chemical Li deintercalation.[38]

Such blockage of cationic redox is more important in the M = Cr case (Figure 2b); now the Cr 3d orbitals are lower-lying than the top of S^{2-} 3p band,[36] so charge balance of the hypothetical CrS_2 phase requires oxidation of S^{2-} anions. If it were attainable, its likely theoretical formulation would be $Cr^{3+}[S^{2-}][S^-]$, with the creation of holes at the top of the S^{2-} 3p band. In reality, such anionic oxidation was not possible even by soft-chemical Li deintercalation from $LiCrS_2$. However, DiSalvo et al. reported full delithiation of the alloyed system $Li_xCr_yV_{1-y}S_2$ ($0 \le x \le 1$ and $0 \le y \le 0.75$),[39] and Goodenough et al. rationalized activation of anionic redox in this Cr-rich system (e.g., $y = 0.75$) by the "pinning" effect of

https://doi.org/10.1021/acsorginorgau.3c00043
ACS Org. Inorg. Au 2024, 4, 26−40

hybridization between the V 3d band and the top of the S^{2-} 3p band to facilitate creation of anionic sp holes.[36,40] The same explanation could be applied to the thiospinel $CuCr_2S_4$; its formal charge balance was considered to be $[Cu^+]$-$[Cr^{3+}]_2[S^{2-}]_3[S^-]$ with holes in the S 3p band that work as redox centers during intercalation of additional Cu,[41] but those anionic sp holes might actually be hybridized with itinerant $Cu^{2+/+}$ couple.[36] The concept of "pinning", i.e., hybridization of cationic and anionic redox couples around a Fermi level, has been applied to design next-generation cathode materials pursuing cumulative electrochemical capacity from both cationic and anionic redox. Fe^{2+} doping greatly improved the electrochemical performance of Li-rich layered sulfide Li_2TiS_3[42] and so does Ni^{2+} doping in the oxide variant Li_2MnO_3,[43] through possible pinning of $S^{2-/-}$ and $O^{2-/-}$ bands. Such hybridization was found effective particularly in Li-rich oxides since it might prevent oxidized $O^{2-/-}$ anions being condensed into gaseous O_2 molecules.[44]

By going further along the periodic table toward late transition metals (M = Mn, Fe, Co, Ni etc..), anionic sp holes become no longer itinerant and are condensed into covalent chalcogen-chalcogen bonds[34,40] (Figure 2b). This leads to the occurrence of pyrite- or marcasite-type structures with the expected $M^{2+}[Ch_2]^{2-}$ charge balance, where chalcogen sp bands are split into molecular orbital levels of $[Ch_2]^{2-}$ dimers. These $[Ch_2]^{2-}$ dimers should be, in principle, able to accept additional electrons into their antibonding σ^* level leading to reductive cleavage of the dimers as in Figure 1b. However, those 3D compounds without a vdW gap tend to undergo alternative nontopochemical structure transformations upon chemical or electrochemical lithiation, giving either Li-M-Ch ternary phases[31] or conversion products MCh_{2-x} + x Li_2Ch.[30,32] Topochemical syntheses involving explicit cleavage or formation of covalent Ch−Ch bonds are rare, apart from some seminal studies of layered materials.

One such example concerns delithiation of the Li_2FeS_2 phase to get a new form of FeS_2. Dugast et al. reported chemical and electrochemical delithiation of Li_xFeS_2 down to x = 0.14 (Figure 3a).[45] Mössbauer, EXAFS[46] and infrared[47] spectra suggested that this almost Li-free FeS_2 phase had Fe^{3+} cations in its tetrahedral site, and the possible coexistence of S^{2-} and S^- anions. The overall charge balance of this metastable FeS_2 can be therefore formulated as $Fe^{3+}S^{2-}[[S_2]^{2-}]_{1/2}$, being distinct from its thermodynamically stable polymorph (i.e., $Fe^{2+}[S_2]^{2-}$ pyrite). This metastable FeS_2 could be brought back to the original precursor Li_2FeS_2 electrochemically,[45−47] through the two-phase domain converting FeS_2 to $LiFeS_2$ with S−S bond cleavage, followed by Li insertion into $Li_{2-x}FeS_2$ solid solution involving $Fe^{2+/3+}$ cationic redox (Figure 3b).

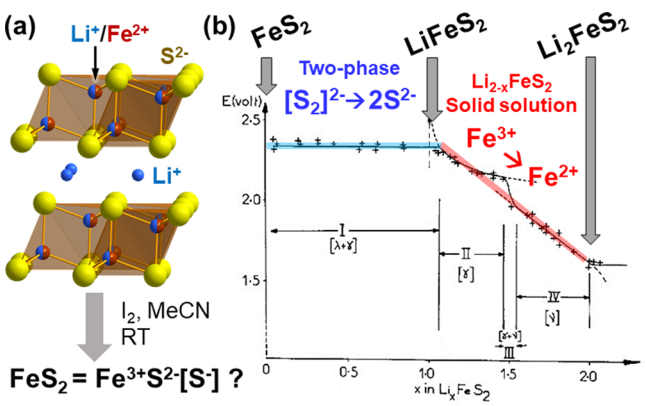

Figure 3. (a) Structure of Li_2FeS_2 and its chemical deintercalation. (b) Quasi-equilibrium discharge curve of metastable FeS_2 prepared by Li deintercalation of Li_2FeS_2. Reprinted with permission from ref 45. Copyright (1981) Elsevier.

These results affirmed the topochemical nature of $LiFeS_2 \leftrightarrow Fe^{3+}S^{2-}[[S_2]^{2-}]_{1/2}$ conversion, and it marked one of the earliest anionic redox topochemical examples that demonstrated its usefulness in the design of new structure types. While it is clearly evidenced that the metastable FeS_2 has a unique structure distinct from those of pyrite or marcasite, its structure has not yet been experimentally solved yet. Some recent experimental[48] and theoretical studies[49] revisited this topochemistry and proposed possible structure models that appear largely plausible (see also the section "Perspectives in Syntheses and Characterizations" later in the article). However, none of these studies reached decisive evidence supporting one proposed structure over the others, leaving room for future comprehensive investigations.

Early transition metals have cationic d bands higher than the top of the anionic sp bands of chalcogen anions, favoring the coexistence of M^{4+} cations and fully reduced Ch^{2-} anions in the MS_2 phase system (Figure 2b). On the other hand, when further Ch anions are added to form MCh_3 or MCh_4 compositions, their anionic sp bands are oxidized into molecular orbital levels of $[Ch_2]^{2-}$ dimers. In the cases of M = Ti, Zr, and Hf, their transition metal trichalcogenides MCh_3 present 1D chains of MCh_6 trigonal prisms extending along b-axis of its monoclinic cell (Figure 4a).[53] These 1D chains are interconnected by a relatively long bond between M^{4+} cation and an apex Ch^{2-} anion while other two anions at the edge form a $[Ch_2]^{2-}$ dimer, building 2D vdW system with the nominal charge balance $M^{4+}Ch^{2-}[Ch_2]^{2-}$. $NbCh_3$ and $TaCh_3$ (Ch = S, Se) also show similar trigonal prismatic chains, but they are connected in different ways rendering their $MCh^{2-}[Ch_2]^{2-}$ layers more corrugated.[54]

Already in the 1970s, these 2D vdW polychalcogenides have been examined as host materials of chemical[55] and electrochemical[56] lithiation. Their reactions with n-butyllithium intercalated 3 equiv of Li^+ cations to give Li_3MCh_3 (M = Ti, Zr, Hf, Nb; Ch = S, Se), whose X-ray powder diffraction patterns could be indexed by the original monoclinic cell (See e.g. $ZrSe_3$ in Figure 4a) with expansion along a- and c-axis, but not along b-axis indicating the preservation of their 1D chain structure. This discovery was followed by extensive experimental[57,58] and theoretical investigations[59] about their structures and reaction mechanisms, as well as application to cathode active materials.[60] Despite these efforts, the structure model proposed for Li_3MCh_3 still remains at the level of a schematic hypothesis inferred from indirect spectroscopic evidence.[58] In general, intercalation in the MCh_3 system led not only to poor crystallinity of the products but also to competing side reactions such as conversion processes (e.g., $NbSe_3$ + 2x Li → $NbSe_{3-x}$ + x Li_2Se),[56,61] hampering detailed analyses of their structures.

Some significant progress in this topochemistry has been made very recently. In 2022, Elgaml et al. first demonstrated rigorous structure characterizations of soft-chemically intercalated A_xZrSe_3 (A = K, Rb, Cs and Ca/NH_3) phases.[50] Partial intercalation of alkali metals up to x ∼ 0.4−0.5 resulted in elongation of the Se−Se bonds implying reductive cleavage of

https://doi.org/10.1021/acsorginorgau.3c00043
ACS Org. Inorg. Au 2024, 4, 26−40

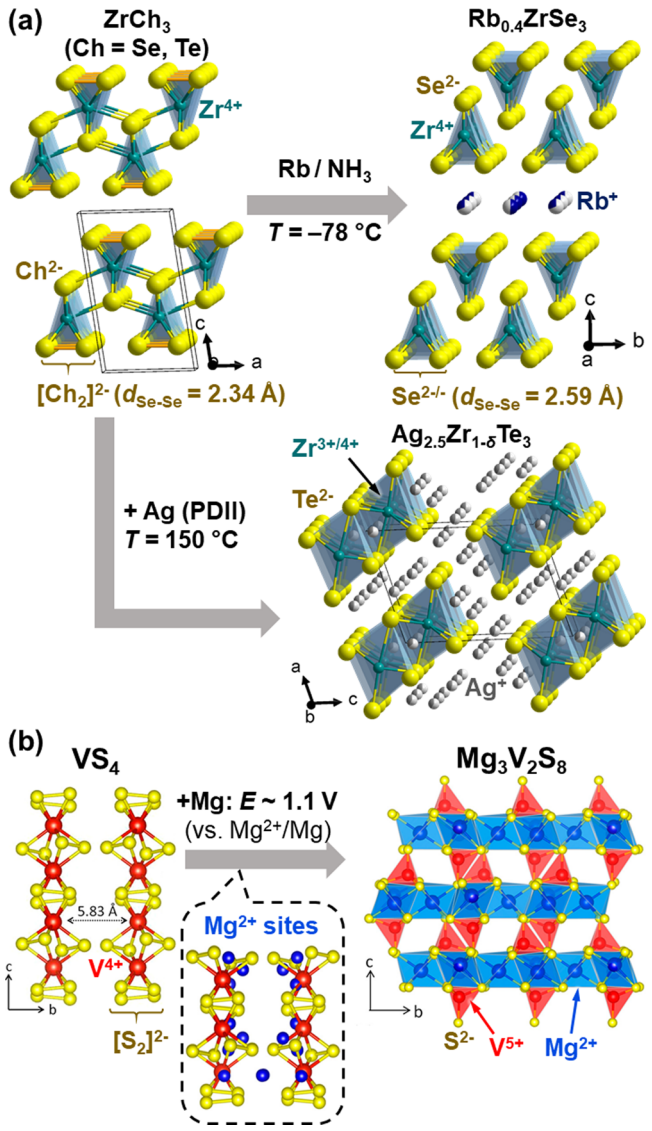

Figure 4. Topochemistry of 2D or 1D vdW polychalcogenides. (a) Intercalation of rubidium[50] and silver[51] into $ZrCh_3$ (Ch = Se, Te) that gave $Rb_{0.4}ZrSe_3$ and $Ag_{2.5}Zr_{1-\delta}Te_3$, respectively. See Figure 10 for proton-driven ion introduction (PDII). (b) Electrochemical intercalation of Mg^{2+} into VS_4 giving $Mg_3V_2S_8$ at $E \sim 1.1$ V (vs Mg^{2+}/Mg). Adapted from ref 52. Copyright (2020) American Chemical Society.

$[Se_2]^{2-}$ dimers, as well as longer interchain $M^{4+}-Se^{2-}$ distances (Figure 4a). Further extent of metal intercalation was achieved by Fujioka et al.[51] using their newly developed synthesis method, coined a Proton-Driven Ion Introduction (PDII; see also the section "Perspectives in Syntheses and Characterizations" later in the article). This electrochemical intercalation using solid electrolytes successfully introduced Ag^+ cations into $ZrTe_3$ up to 2.5 equiv, necessarily involving both $Te^{2-/-}$ and $Zr^{3+/4+}$ redox couples (Figure 4a). Their X-ray and electron diffraction studies clearly showcased its gradual transition from 1D trigonal prismatic chains to dimeric octahedral chains through the formation of quasiamorphous phases, where long-range order was lost, except along the 1D chains.

VS_4 is another variant of early transition metal polychalcogenides, but in this case all sulfur anions are oxidized to $[S_2]^{2-}$ dimers comprising 1D vdW chains of VS_8 square antiprisms (Figure 4b).[62] VS_4 recently regained attention from electrochemists since its mixture with reduced graphene oxides (rGO) showed excellent performance as a cathode of Li-, Na-, and Mg-ion secondary batteries.[63,64] Their electrode reactions were then found to go through the ternary Li_3VS_4 or $Mg_3V_2S_8$ phases with V^{5+} and S^{2-} species before reaching their conversion products V^0 + Li_2S or MgS.[65,66] However, the structures of these possible intercalate compounds had remained unsolved due to the poor crystallinity of the products. In 2020, Dey et al. combined computational structure prediction and total scattering analyses to identify the structure of this $Mg_3V_2S_8$ phase (Figure 4b),[52] which displayed a strong structural filiation with the parent VS_4 phase.

The host materials addressed above have vdW gaps in their structures, and thus, their topochemistry may be categorized as a variant of classic intercalation processes (Figure 1a). Nevertheless, it was clear from the recent examples shown in Figure 4 that the reductive cleavage of covalent anion−anion bonds triggered unique structure transformations. Structure characterization was too challenging when those intercalation compounds were first identified, but today it becomes increasingly feasible by employing modern synthetic and characterization tools. This trend is an encouraging sign for future materials designs through anionic redox topochemistry.

"ZIPPER"-TYPE TOPOCHEMISTRY BASED ON ANIONIC REDOX

(1) Intercalation of Metal Cations

In 2017, we proposed to make a use of anionic redox topochemistry for design of layered materials.[26] Anionic redox involves the formation or cleavage of anion−anion bonds. As depicted in Figure 1b, this anionic redox enables a special type of structure transformation when the anion−anion bonds link host cationic layers. Upon the redox reaction with external metal species, those anion−anion linkers are reductively cleaved, opening up a space to accommodate metal intercalants between host cationic layers. This process resembles opening a zipper made of anion−anion bonds, enabling construction of new layered materials from non-vdW polychalcogenides.

The proof-of-concept experiments of this novel topochemistry were first performed on $La_2O_2S_2$ and $Ba_2F_2S_2$, the compounds where redox-inert, host cationic $[La_2O_2]^{2+}$ or $[Ba_2F_2]^{2+}$ slabs are interconnected by anionic $[S_2]^{2-}$ dimers (Figure 5a). Our recent DFT calculation revealed that sulfur 3sp bands in these compounds were split into respective molecular orbital levels of $[S_2]^{2-}$ dimers[67,68] in a similar way to the MnS_2 case shown in Figure 2b, leaving one antibonding σ^* orbital available for redox reaction with external reducing agents. Accordingly, if metal intercalants M^0 are sufficiently reducing to donate their electrons to the σ^* level of $[S_2]^{2-}$ dimers, then these non-vdW host materials should have their S−S bonds broken to accommodate metal intercalants M^{n+}.

To verify this, $La_2O_2S_2$ and $Ba_2F_2S_2$ were heated with Cu^0 powder in pressed pellets, at low temperature (T = 250−275 °C), where conventional precursors without $[S_2]^{2-}$ dimers could not produce the intercalated quaternary phases (Figure 5a).[26,69] The reaction swiftly proceeded within a few hours with an intermediate grinding, giving $[La_2O_2]^{2+}[Cu_2S_2]^{2-}$ or $[Ba_2F_2]^{2+}[Cu_2S_2]^{2-}$ phases, where S−S bonds were cleaved and 2D copper sulfide layers were formed. Equally, the successful intercalation of Cu was confirmed under solvother-

https://doi.org/10.1021/acsorginorgau.3c00043
ACS Org. Inorg. Au 2024, 4, 26−40

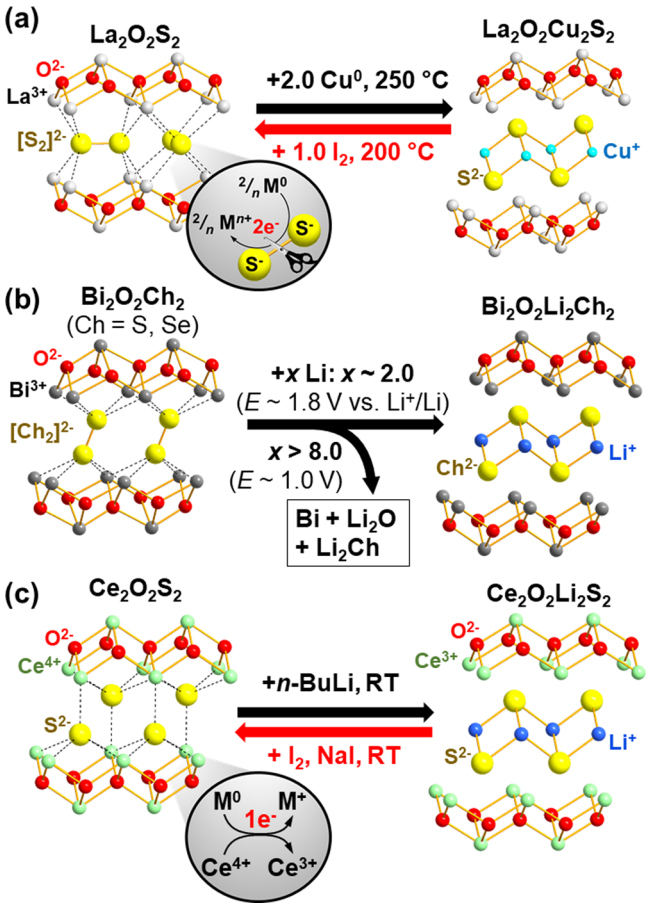

Figure 5. (a) Chemical intercalation of Cu[26] into $[La_2O_2]^{2+}[S_2]^{2-}$ and (b) electrochemical intercalation of Li into $[Bi_2O_2]^{2+}[Ch_2]^{2-}$ (Ch = S, Se) that was in competition with nontopochemical conversion.[71] (c) Chemical lithiation of $[Ce_2O_2]^{4+}[S^{2-}]_2$ driven by cationic $Ce^{3+/4+}$ redox.[72]

mal (Reagent: CuCl + ethylenediamine producing Cu^0 through disproportionation, T = 200 °C) and mechanochemical (Reagent: Cu^0 powder, planetary ball milling at 800 rpm, 20 min ×2) conditions.[69]

Furthermore, Cu could be deintercalated upon the reaction with I_2 at 200 °C, recovering the original polysulfide precursor $La_2O_2S_2$ by oxidation of the S^{2-} anions.[26] Such reversibility and mild reaction conditions affirm the topochemical nature of those structure transformations.

This reductive intercalation of Cu was then examined in various host materials,[26,70] ranging from the simple binary disulfides $Ba^{2+}[S_2]^{2-}$ to its homologue $Ba^{2+}[S_3]^{2-}$ built of sulfur trimers as well as the selenide system $[La_2Se_2]^{2+}[Se_2]^{2-}$. In all of these cases, the low-temperature solid−solid reactions with Cu^0 powder produced copper chalcogenides: $BaCu_2S_2$, $BaCu_4S_3$, and $LaCuSe_2$ (= $[La_2Se_2]^{2+}[Cu_2Se_2]^{2-}$).

As for oxidative deintercalation, Chaupatnaik et al. recently reported the removal of Cu^+ cations from $[Bi_2O_2]^{2+}[Cu_2Ch_2]^{2-}$ (Ch = S, Se), being isostructural with $La_2O_2Cu_2S_2$, using I_2 in acetonitrile solution.[71] This reaction at room temperature (RT) gave the novel layered polychalcogenides $[Bi_2O_2]^{2+}[Ch_2]^{2-}$, which were further confirmed to undergo both chemical and electrochemical intercalation of Li^+ cations (Figure 5b). At further negative potential, this electrochemical lithiation was followed by nontopochemical conversion process, leading to destruction of their overall layered structure: $Bi_2O_2Li_2Ch_2 + 6\ Li^+ + 6\ e^- \rightarrow 2\ Bi^0 + 2\ Li_2O + 2\ Li_2Ch$. Such competition between topochemical lithiation and non topochemical conversion was commonly observed in various polychalcogenide systems (e.g., $FeCh_2$, $NbSe_3$ and VS_4).[30−32,61,65]

This anionic redox topochemistry resembling a "zipper" may be best contrasted with that of $Ce_2O_2S_2$, which was recently prepared from $Ce_2O_2Ag_{1.6}S_2$ by Cassidy et al. using an acetonitrile solution of I_2 and NaI.[72] $Ce_2O_2S_2$ contains lanthanide oxide layers similar to those in $La_2O_2S_2$, but its Ce cations took the oxidation state of +4 with the [Xe] $4f^0$ configuration and its formal charge balance formulated as $[Ce_2O_2]^{4+}[S^{2-}]_2$. Accordingly, there were no longer covalent anion−anion bonds that "zipped up" host cationic slabs (Figure 5c). When this compound was subject to chemical and electrochemical lithiation, $Ce^{3+/4+}$ cations played the role of redox center while S^{2-} anions remained redox inert throughout the process.

It is also possible to switch from cationic to anionic redox in the same system. $Sr_2MnO_2Cu_{1.5}Ch_2$ (Ch = S, Se), a layered compound where the perovskite type Sr_2MnO_2 slabs are intergrown with the anti-PbO type $Cu_{1.5}Ch_2$ slabs, is one of such compounds displaying complex redox competition (Figure 6). As shown in Figure 2b, Mn cations take the +2 oxidation state in pure chalcogenides and further oxidation takes place rather at anionic Ch^{2-} 3sp bands.[34] On the other hand, Mn cations in $Sr_2MnO_2Cu_{1.5}Ch_2$ were found to exhibit the higher oxidation state at +2.5, owing to heteroleptic coordination of their MnO_4Ch_2 octahedra.[75] This higher-lying Mn 3d band was actually subjected to further oxidation during the partial deintercalation of Cu from $Sr_2MnO_2Cu_{1.5}S_2$. Its reaction with I_2 in acetonitrile solution removed ca. 10% of Cu^+ cations from the host framework, giving $Sr_2MnO_2Cu_{1.34(1)}S_2$ with an incommensurately modulated structure (Figure 6, top).[73] X-ray absorption spectra and magnetometry analyses confirmed the oxidation of $Mn^{2+/3+}$ cations, and this cationic redox altered antiferromagnetic ordering within its MnO_2 square network from CE-type to an alternative pattern of ferromagnetic stripes.

Cu^+ cations could not be removed beyond 10% from those oxychalcogenides neither at higher temperature than 0 °C nor by using stronger oxidizing agents such as Br_2 or NO_2BF_4 that led to overall decomposition. Such greater extents of deintercalation required the multistep route going through Cu−Li exchange and subsequent dissolution of the surface Cu^0 metals (Figure 6 bottom).[74] Those steps gave $Sr_2MnO_2Li_xCh_2$ as the synthetic intermediate, which was then subject to Li^+ deintercalation by using the organic molecules carrying S−S bonds as oxidizing agents. This oxidative deintercalation at T = 80 °C activated anionic $Ch^{2-/-}$ redox, to transform the anti-PbO type Li_xCh_2 slabs into 2D array of Ch_2 dimers. X-ray absorption and magnetometry data indicated that $Mn^{2+/3+}$ cations of the final product were oxidized to a lesser extent than $Sr_2MnO_2Cu_{1.34}S_2$ even though a much larger amount of the monovalent metal in the chalcogenide layer had been removed. In contrast, oxidation of its Ch^{2-} anions was clearly evidenced by the pre-edge feature of their X-ray absorption near-edge structure (XANES) as well as Raman peaks corresponding to Ch−Ch stretching modes.

These contrasting results arising from different routes suggested tight competition between cationic $Mn^{2+/3+}$ redox and anionic $Ch^{2-/-}$ redox. As long as the oxidation state of $Mn^{2+/3+}$ cations does not deviate far from its original value

https://doi.org/10.1021/acsorginorgau.3c00043
ACS Org. Inorg. Au 2024, 4, 26−40

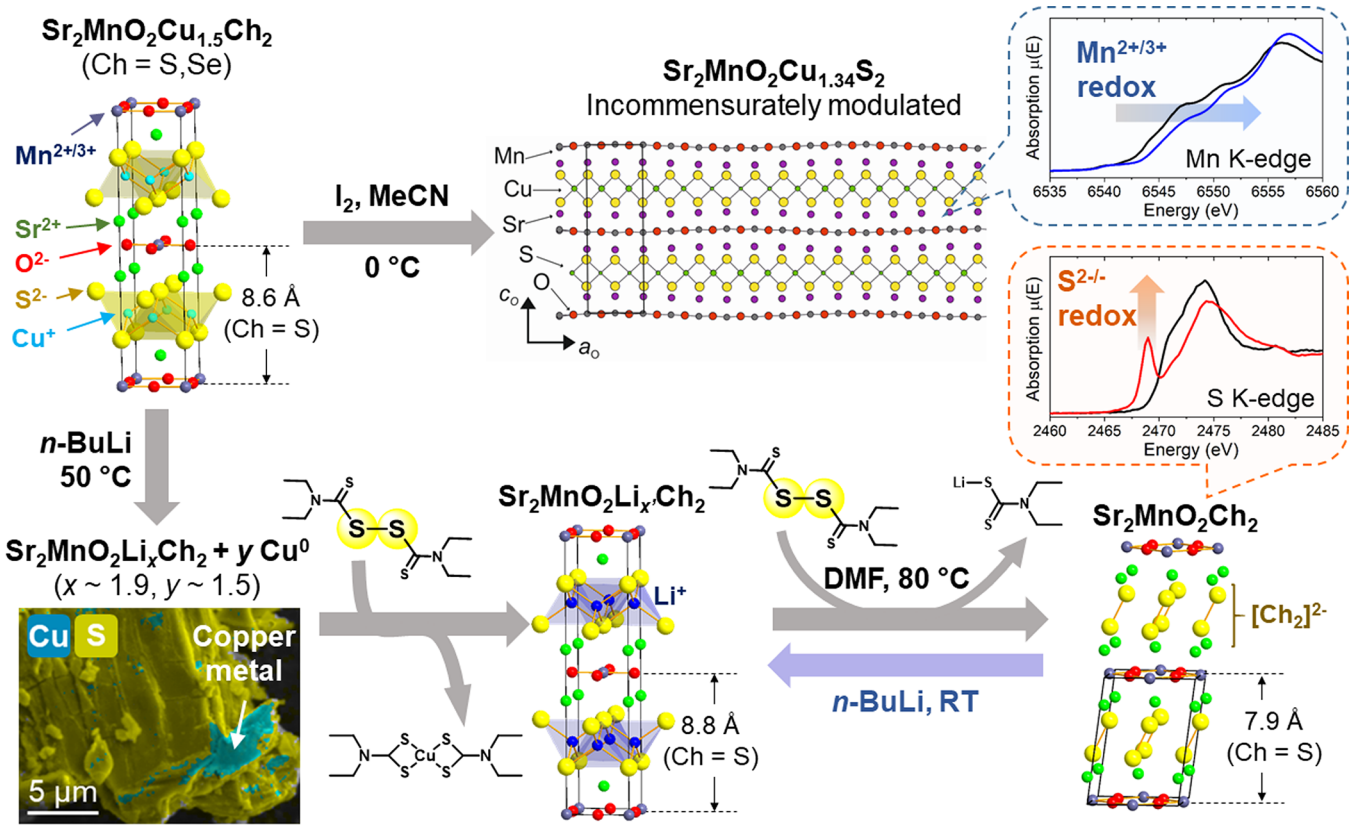

Figure 6. Topochemistry of $Sr_2MnO_2Cu_{1.5}Ch_2$ (Ch = S, Se). (Top) Partial deintercalation of Cu^+ cations from the Ch = S system using I_2. The structure of its product $Sr_2MnO_2Cu_{1.34}S_2$ was reprinted with permission under a Creative Commons Attribution 3.0 from ref 73. Copyright (2015) AIP Publishing. Mn K-edge XANES spectra (black: precursor; blue: product) indicated that the partial deintercalation led to oxidation of $Mn^{2+/3+}$ cations. (Bottom) Multistep topochemistry starting from reductive Cu−Li exchange (image: SEM/EDX map evidencing extrusion of the surface Cu^0 metals), followed by Cu dissolution and subsequent Li^+ deintercalation at elevated temperature (T = 80 °C). S K-edge XANES (black: precursor, red: product) indicated $S^{2-/-}$ oxidation in the final product. The bottom scheme was adapted with permission under a Creative Commons Attribution 4.0 from ref 74. Copyright (2023) Springer Nature.

+2.5, (de)intercalation changes the electron count of Mn 3d bands. However, once a greater extent of deintercalation imposes further oxidation, it triggers $Ch^{2-/-}$ redox, keeping the oxidation state of Mn at around +2.5. Similar redox competition was observed also during electrochemical Cu−Li exchange of $Sr_2MnO_2Cu_{3.5}S_3$, a structural homologue of $Sr_2MnO_2Cu_{1.5}Ch_2$ with the thicker copper sulfide layers.[76] Those observation may be related to redox competition during Mg^{2+} intercalation into VS_4 (See Figure 4b),[52,64] where reduction of its $[S_2]^{2-}$ dimers coincided with oxidation of its V^{4+} cations to V^{5+}. To unlock the full picture of this complex redox behavior, it is necessary to carry out further in-depth analyses about how their electronic structures evolve during (de)intercalation processes.

The first preliminary successes in this "zipper"-type topochemistry have been limited mainly to intercalation of monovalent cations (e.g., Li^+ and Cu^+). It would be then the next major challenge to extend the scope of intercalants to divalent or trivalent cations, especially to those with open-shell configurations at the d-levels since their interaction will construct 2D transition metal chalcogenides with possible quantum functionalities (Figure 1b).

Some proof-of-concept experiments have been made for this using the simple binary polysulfides.[70] As shown in Figure 7, the structure of $Ba^{2+}[S_2]^{2-}$ has a strong filiation with $BaNiS_2$, the quasi-layered compound built of NiS_5 square pyramids. Accordingly, one can expect that the reductive cleavage of its

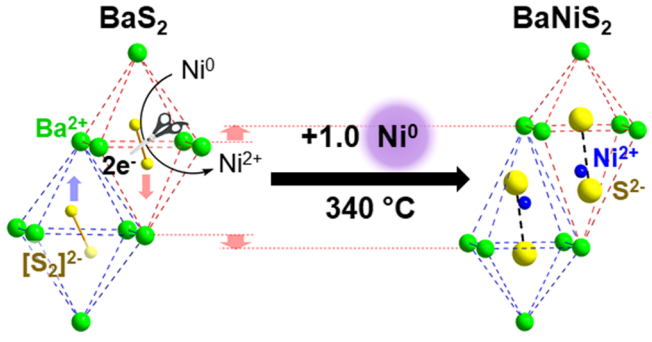

Figure 7. Topochemical structure transformation proposed for low-temperature Ni insertion into $Ba^{2+}[S_2]^{2-}$ giving the quasi-layered $Ba^{2+}[NiS_2]^{2-}$ phase. Reprinted with permission from ref 70. Copyright (2019) Royal Society of Chemistry.

S−S bonds (i.e., $Ni^0 + [S_2]^{2-} \rightarrow Ni^{2+} + 2S^{2-}$) triggers insertion of these Ni^{2+} cations to construct this ternary phase known as the promising spintronic material,[77] with a low kinetic barrier. In practice, the solid−solid reaction between BaS_2 and Ni^0 powders was found to proceed at T = 340 °C, a temperature much lower than the conventional route starting from BaS, Ni and elemental sulfur (T = 800−950 °C).[70] However, this insertion process was in competition with the nontopochemical conversion process $BaS_2 + Ni^0 \rightarrow BaS + NiS$, which had to be suppressed by delicate control of thermal treatments and

https://doi.org/10.1021/acsorginorgau.3c00043
ACS Org. Inorg. Au 2024, 4, 26−40

the use of BaS_3 instead of BaS_2. The similar low-temperature reaction was observed also for BaS_3 and Fe^0 giving $BaFe_2S_3$, which was known as the first spin-ladder iron-based superconductor,[78] but it was also in the competition with the decomposition into other nontopochemical products.[70] These preliminary results have demonstrated the feasibility of constructing low-dimensional quantum materials through the "zipper"-type topochemistry, but at the same time raised the challenge to steer the selectivity between several competing processes.

The examples described thus far have focused primarily on chalcogenides. On the other hand, secondary battery research has been more focused on the redox of oxygen anions.[44] In the 2000s, Li_2MnO_3 doped with Ni and Co, referred to as Li-rich NMC, was found to be an excellent cathode material for a Li-ion secondary battery,[79] with extraordinary capacity arising not only from cationic redox of its transition metals and but also from anionic redox of its oxygen. This discovery prompted electrochemists to study the redox activity of oxygen in Li-rich oxides. To date, topochemistry involving the formation or cleavage of an O−O bond still remains elusive. Nevertheless, recent microscopic[80] and neutron diffraction[81] studies spotted formation of O−O dimers during oxidative Li^+ deintercalation of the Li-rich cathode Li_2IrO_3. This encourages future attempts to design new compounds through the reversible formation of anionic O−O bonds.

Dimerization, oligomerization and polymerization of anionic networks are not limited to group 16 elements, but also known among various semimetals and intermetallic compounds built of pnictogens, carbon group and transition metal elements.[82] Actually, the analogy of "zip-lock" was first used by Bhaskar et al.[27] to refer to topochemistry of LiNiB that involved Ni−Ni bond formation (Figure 8). They discovered that deintercalation of Li^+ cations oxidized its anionic $[NiB]^-$ single layers, leading to its condensation into double $[NiB]_2$ or triple $[NiB]_3$ layers that "zipped up" the spaces between NiB slabs through Ni−Ni bond formations. HAADF-STEM image of the deintercalated product (Figure 8c) highlighted the structural diversity of these zipped-up $[NiB]_n$ (n = 2, 3) layers, heralding future prospects to design various 2D metal borides coined MBenes.

(2) Deintercalation of Sulfur Anions

Reductive cleavage of chalcogen-chalcogen bonds is conducive not only to intercalation of metal cations but also to deintercalation of their chalcogen anions (Figure 1b). As described in Figure 5a, the layered oxysulfide $[La_2O_2]^{2+}[S_2]^{2-}$ reacted with Cu^0 metals to trigger its intercalation, resulting in construction of 2D $[Cu_2S_2]^{2-}$ layers.[26] On the other hand, its low-temperature (T = 350 °C) reaction with Ag^0 metals did not give the corresponding quaternary phase $[La_2O_2]^{2+}[Ag_2S_2]^{2-}$, but instead produced the mixture of Ag_2S and the novel sulfur-deficient $La_2O_2S_{1.5}$ (= $[La_4O_4]^{4+}[S_2]^{2-}[S^{2-}]$) phase.[28] 3D electron diffraction analysis solved the structure of this novel phase (Figure 9a); *oA*-$La_2O_2S_{1.5}$ (*oA*: Pearson's notation) crystallizes in the *Amm*2 space group, where one-fourth of the sulfur anions were removed through cleavage of some of the S−S bonds. Throughout the process, the PbO-type $[La_2O_2]^{2+}$ slabs retained their structural integrity, indicating the topochemical nature of this sulfur deintercalation.

This discovery encouraged us to go further on sulfur deintercalation. La_2O_2S is the x = 1 end member of the

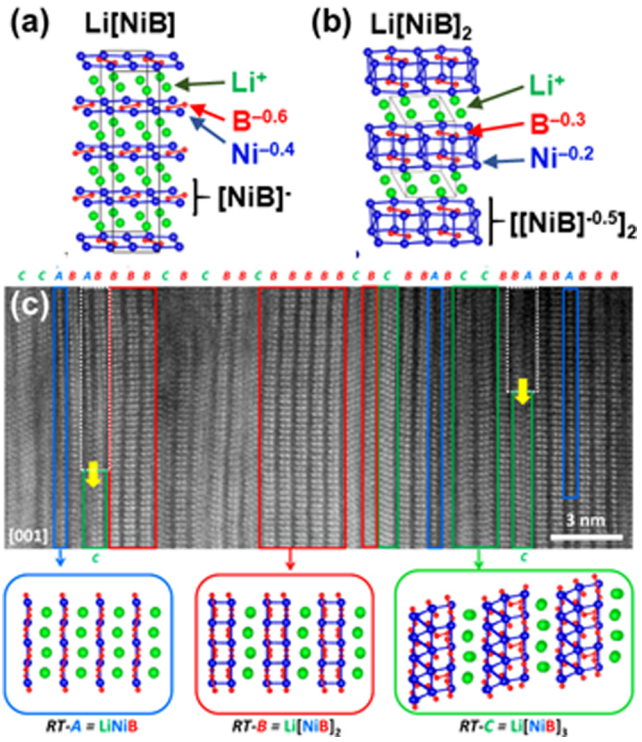

Figure 8. (a) Room-temperature (RT) polymorph of LiNiB and (b) its deintercalated phase $Li[NiB]_2$. Net charges were estimated by Bader analysis. (c) HAADF-STEM image of the product after deintercation, highlighting the coexistence of the pristine LiNiB slabs (RT-A), the deintercalated $Li[NiB]_2$ double layers (RT-B) and $Li[NiB]_3$ triple layers (RT-C). Reprinted from ref 27. Copyright (2021) American Chemical Society.

$La_2O_2S_{2-x}$ series and belongs to one of the most well-known oxysulfide family Ln_2O_2S (Ln = rare-earth elements except Sc and *Pm*). They have been serving as excellent matrices for phosphor dopants and found in various applications ranging from cathode ray tubes, laser emission/absorption, scintillators to bioimaging.[83] This known La_2O_2S phase could be prepared simply by desulfurizing $La_2O_2S_2$ under 5% H_2/Ar flow under 350 °C,[28] but its hexagonal structure (*hP*-La_2O_2S in Pearson's notation) with the $P\bar{3}m1$ space group no longer retained the quasi-tetragonal $[La_2O_2]^{2+}$ slabs of $La_2O_2S_2$ (Figure 9b). On the other hand, our computational structure prediction using the evolutionary algorithm USPEX[84] have suggested, besides the most stable *hP*-La_2O_2S, another polymorph with the space group *Amm*2. This metastable polymorph, namely, *oA*-La_2O_2S, has the quasi-tetragonal PbO-type $[La_2O_2]^{2+}$ slabs common with $La_2O_2S_2$. To reach this hypothetical metastable phase, $La_2O_2S_2$ was treated with Rb^0, an alkali metal sufficiently reducing to cut all S−S bonds but too large to be inserted into the host framework.[28] The reaction proceeded quickly at 200 °C to give the predicted *oA*-La_2O_2S phase, whose HAADF-STEM image clearly evidenced PbO-type $[La_2O_2]^{2+}$ slabs inherited from $La_2O_2S_2$ (Figure 9c).

As expected from their topochemical relationship, both *oA*-$La_2O_2S_{1.5}$ and *oA*-La_2O_2S could be brought back to $La_2O_2S_2$ by treating with sulfur at 200 °C. This reversible (de)intercalation chemistry is not limited to the lanthanum system but was recently extended to other $Ln_2O_2S_2$ (Ln = Pr, Nd) precursors, which reacted readily with alkali metals to give the sulfur-deintercalated *oA*-Ln_2O_2S phases.[85]

https://doi.org/10.1021/acsorginorgau.3c00043
ACS Org. Inorg. Au 2024, 4, 26−40

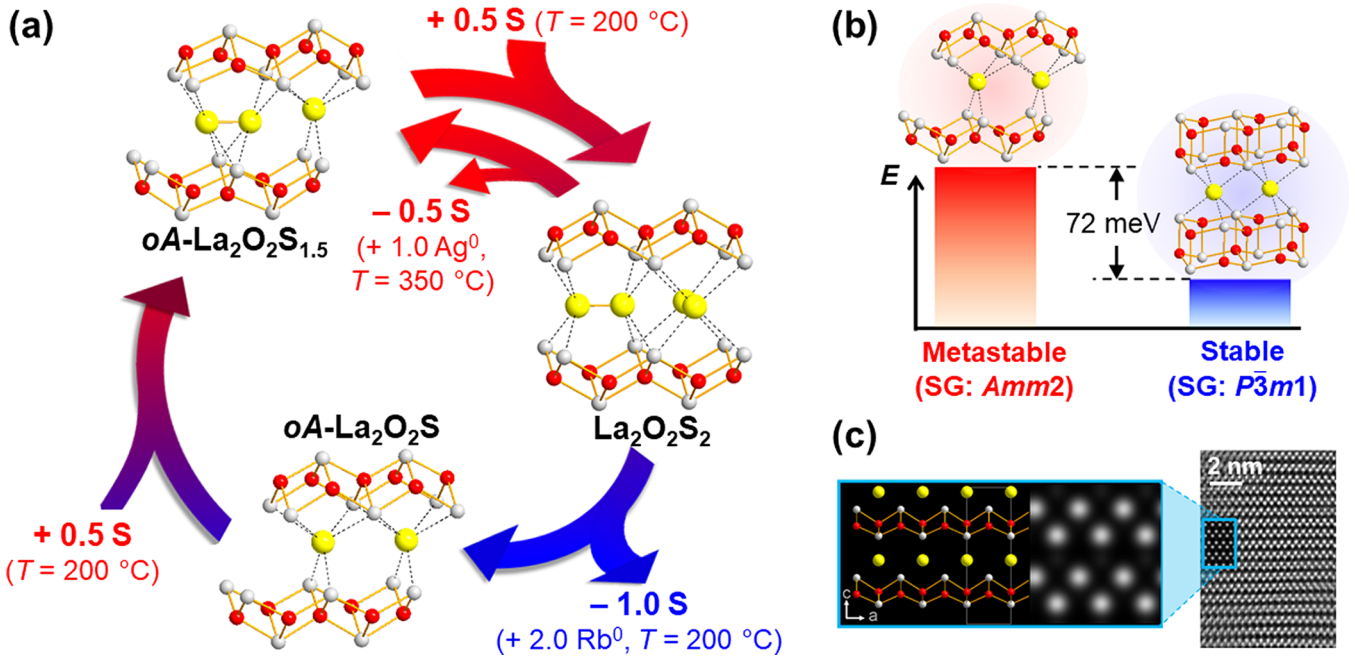

Figure 9. (a) Topochemical deintercalation of sulfur anions from layered oxysulfide $[La_2O_2]^{2+}[S_2]^{2-}$. Reaction conditions of respective processes are noted in parentheses. (b) Two possible structures and their relative energies predicted by computational structure prediction. (c) HAADF-STEM image after the reaction with Rb^0. It displayed good agreement with the simulated image of the *oA*-La_2O_2S model. Reprinted with permission under a Creative Commons Attribution 4.0 from ref 28. Copyright (2021) Springer Nature.

Table 1. Metastable Compounds Discovered Using Anionic Redox Topoichemistry

product	precursor	synthesis method	redox center	reaction type	literature
Li_3MCh_3[a]	MCh_3 (M = Ti, Zr, Hf, Nb; Ch = S, Se)	chemical, electrochemical	$M^{3+/4+}$, $Ch^{2-/-}$	metal intercalation into quasi-1D vdW system	55−60
$Rb_{0.4}ZrSe_3$	$ZrSe_3$	chemical	$Se^{2-/-}$	metal intercalation into quasi-1D vdW system	50
$Ag_{2.5}Zr_{1-\delta}Te_3$	$ZrTe_3$	electrochemical	$Zr^{3+/4+}$, $Te^{2-/-}$	metal intercalation into quasi-1D vdW system	51
$Mg_3V_2S_8$	VS_4	electrochemical	$V^{4+/5+}$, $S^{2-/-}$	metal intercalation into 1D vdW system	52
metastable 2D FeS_2[a]	Li_2FeS_2	chemical, electrochemical	$Fe^{2+/3+}$, $S^{2-/-}$	metal deintercalaion to form 2D vdW system[b]	45−49
$Sr_2MnO_2Ch_2$	$Sr_2MnO_2Cu_{1.5}Ch_2$ (Ch = S, Se)	chemical	$Ch^{2-/-}$	"zipper"-type deintercalation of metal cations	74
$Bi_2O_2Ch_2$	$Bi_2O_2Cu_2Ch_2$ (Ch = S, Se)	chemical, electrochemical	$Ch^{2-/-}$	"zipper"-type deintercalation of metal cations	71
$Li[NiB]_n$ (n = 2, 3)	LiNiB	chemical	$[NiB]^-/[NiB]^{-1/n}$	"zipper"-type deintercalation of metal cations	27
$Ln_2O_2S_{2-x}$ (x = 0.5, 1.0)[c]	$Ln_2O_2S_2$ (Ln = La, Pr, Nd)	chemical	$S^{2-/-}$	"zipper"-type deintercalation of chalcogen anions	28, 85

[a]Structures of those products have not been fully identified yet. [b]According to the proposed structures reported in refs 48,49. [c]La_2O_2S (the end member at x = 1.0) crystallized in the metastable polymorph with *Amm*2 space group. See Figure 9 for details.

Those are the first successful syntheses of novel metastable compounds through the low-temperature deintercalation of sulfur anions. Compared to oxygen or fluorine anions, insertion and removal of the bulky chalcogen anions are more likely to end up with nontopochemical, destructive structure transformations. However, there are several inspiring reports supporting the feasibility of sulfur (de)intercalation chemistry. One such example is the high-temperature topochemistry of $Cs_2[Ga_2[Ch_2]_{2-x}Ch_{2+x}]$ (Ch = S, Se; x = 0, 1, 2) reported by Friedrich et al.[86,87] They studied thermal decomposition behaviors of the 1D selenogallate $Cs_2[Ga_2[Ch_2]_2Ch_2]$ (= $CsGaCh_3$), where $GaCh_4$ tetrahedra share vertexes and are further connected by anionic Ch−Ch bonds at another apex. Those 1D polychalcogenides underwent decomposition into $Cs_2[Ga_2[Ch_2]Ch_3]$ (= $Cs_2Ga_2Ch_5$) and $Cs_2[Ga_2Ch_4]$ (= $CsGaCh_2$) at 540−680 °C (Ch = Se)[86] and 440−540 °C (Ch = S).[87] The products of the thermal decomposition retained the 1D chain structure of $GaCh_4$ tetrahedra, but their Ch−Ch bonds were broken, and half of their chalcogen anions were deintercalated from the system. In the case of Ch = Se, the deintercalation could be reversed through the reaction with elemental Se at 500−600 °C, implying the topochemical nature of the process.

Another intriguing example can be found in nature. Lapis lazuli, or its ground form, ultramarine, is a metamorphic rock famous for its bright blue color. The blue color is known to come from the presence of $[S_3]^-$ radical anions embedded in β-cages of its zeolite LTA framework,[88] and this sulfur-

https://doi.org/10.1021/acsorginorgau.3c00043
ACS Org. Inorg. Au 2024, 4, 26−40

containing component can be formulated as $Na_6(Al_6Si_6O_{24})\cdot 2NaS_x$ (x = 2−3; note that bulk compositions of ultramarines are much more complex containing, e.g., Ca SO_4, Cl, and OH ions). Actually, these blue $[S_3]^-$ species in β-cages could be enriched by heating with elemental sulfur[89] or under dynamic vacuum.[90] These observations suggested the migration of sulfur anions in the zeolite framework.

Except for the few cases described here, sulfur anions are generally reckoned to be an immobile species in solids, and their solid-state diffusion is scarcely documented. Nevertheless, Ushakova and co-workers carried out a series of attempts to evaluate diffusion constants of S^{2-} anions in solid electrolytes using Hebb-Wagner type cells[91] and other electrochemical setups.[92] According to their reports, several ternary sulfides ALn_2S_4 (A = Ca, Ba; Ln = Sm, Gd, Yb) exhibited faster S^{2-} diffusion when doped with the binary sulfides Ln_2S_3, and the activation energy of S^{2-} diffusion could be much lower than 1.0 eV.[91] This possible $Ch^{2-/-}$ diffusion was corroborated by the recent report from Lei et al.;[93] they demonstrated electrochemical (de)intercalation of $Se^{2-/-}$ anions in between vdW gap of 2D $MoSe_2$. Those results encourages further in-depth analyses from methodological and theoretical viewpoints,[94] as well as possible applications to electrochemical devices based on sulfur-ion shuttling,[95] similar to fluoride-ion batteries that have attracted much recent attention.[96]

PERSPECTIVES IN SYNTHESES AND CHARACTERIZATIONS

Compared to the number of functional materials[3−22] discovered by cationic redox topochemistry, there are still only a handful of examples in which novel compounds were synthesized through topochemistry involving anion−anion bond cleavage or formation (Table 1). One of the major reasons for the scarcity is the complex reaction manifolds of anionic redox topochemistry where multiple side reactions compete with each other.

Already in early studies during the 1970s, competition between metal intercalations (e.g., $MCh_3 + xA \rightarrow A_xMCh_3$; A = alkali metals, M = transition metals) and conversion reactions (e.g., $MCh_3 + 2xA \rightarrow MCh_{3-x} + xA_2Ch$) have been recognized.[7,56] To date, there is no universal strategy to control this competition, but here, we note some synthetic methods that led to successful isolation of the metal-intercalated products suppressing the competing conversion processes.

One viable strategy to harness the competition is electrochemical syntheses since they regulate the introduction of metal intercalants and can be used to avoid progression to conversion reactions. Such control of electrochemical reductions successfully gave new compounds via Mg intercalation into VS_4 (Figure 4b)[52] and Li intercalation into $Bi_2O_2Ch_2$ (Figure 5b).[71] While host materials in those electrochemical syntheses were in powder form and mixed with carbon compounds, Fujioka et al. prepared single crystalline Ag-intercalated $ZrTe_3$ (Figure 4a).[51] They developed the novel method for solid-state intercalation called proton-driven ion introduction[97] (PDII; see Figure 10), where a high voltage between the needle-shaped anode and carbon cathode ionized a hydrogen atmosphere, followed by bombardment of H^+ ions onto a AgI surface, driving Ag^+ cations toward $ZrTe_3$ at the cathode. As a consequence, $ZrTe_3$ respectively received Ag^+ from the AgI electrolyte and electrons from the cathode, producing Ag_xZrTe_3 without destroying its single-crystalline

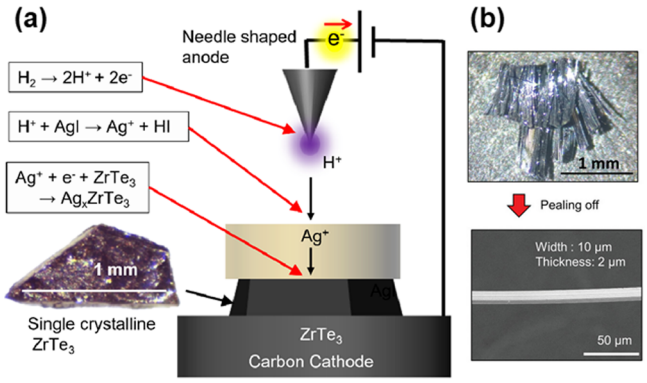

Figure 10. (a) Schematic illustration of proton-driven ion introduction (PDII) used for Ag^+ intercalation into $ZrTe_3$ described in Figure 4a. (b) Photographs of the as-prepared sample after Ag intercalation and the fibrous crystal peeled off from them. Reprinted with permission from ref 51. Copyright (2023) Wiley-VCH.

morphology. Thanks to this, the superconducting behavior of Ag_xZrTe_3 single crystals could be evaluated as a function of Ag content x. Such single-crystal-to-single-crystal (SCSC) routes[98] may be beneficial also for suppressing conversion process given the recent *in situ* TEM study by Luo et al.;[61] they found that Li intercalation into $NbSe_3$ was favored over a competing conversion process in the large crystals while the opposite was observed with small crystals. Those results encourage further comprehensive investigations of the relationship between crystal morphology and the selectivity of the anionic redox topochemistry.

Soft-chemical processes are an alternative approach to isolating intercalation compounds. Traditionally, *n*-butyllithium was employed for chemical lithiation[7] while I_2, Br_2 and NO_2BF_4 were used for oxidative deintercalation.[38,72] The use of I_2 was found effective also for anionic redox topochemistry, as exemplified by deintercalation of Li^+ from $LiFeS_2$ (Figure 3)[45] and Cu^+ from $La_2O_2Cu_2S_2$ and $Bi_2O_2Cu_2Ch_2$ (Ch = S, Se; Figure 5).[26,71] Nevertheless, those oxidizing reagents sometimes led to decomposition of host materials such as $Sr_2MnO_2Cu_{1.5-x}Ch_2$.[73] In this case, undesirable side reactions may be circumvented, as described in Figure 6, by going through reactive intermediate (e.g., $Sr_2MnO_2Li_xCh_2$) and by employing chemoselective reagents (e.g., Difulfiram for $S^{2-/-}$ oxidation).[74] Such multistep syntheses through energetic intermediates are a part of routine practices in organic chemistry, and are increasingly recognized as an important strategy also in solid-state chemistry (see, e.g., refs 99 and 100 where insertion of H^+ or H^- ions rendered host oxide frameworks less stable, enabling more challenging topochemical transformations).

This section highlights a few soft-chemical routes successfully used in the reported cases (see Table 1). However, many other synthesis methods could potentially be applied to control anionic redox topochemistry. For instance, metathesis reactions have often been utilized in syntheses of polychalcogenides.[101] These reactions can therefore serve as a driving force for introducing chalcogen-chalcogen bonds in a topochemical manner. Indeed, metathesis reactions have successfully introduced chalcogen anions in between the host cationic slabs, resulting in $[Hf_2N_2]^{2+}[S^{2-}]$ from $[Hf_2N_2]^{2+}[Cl^-]_2$ and Ti_3C_2Ch (Ch = S, Te) from $Ti_3C_2Br_2$ MXene.[102,103] While these examples did not involve anionic redox, this alternative driving force may provide an opportunity

https://doi.org/10.1021/acsorginorgau.3c00043
ACS Org. Inorg. Au 2024, 4, 26−40

to expand the applicability of chalcogen (de)intercalation beyond the *oA*-$Ln_2O_2S_{2-x}$ system described in Figure 9.

Structure characterization is another major challenge in anionic redox topochemistry. Generally speaking, anion−anion bond formation and cleavage resulted in relatively poor crystallinity of the topochemical products. Two seminal examples, Li-intercalated Li_xMS_3 (M = Ti, Zr, Hf; $x \sim 3$) and the metastable FeS_2 from Li deintercalation of Li_xFeS_2 (see Figure 3), were both reported over 40 years ago,[45,55] but their structures could not be solved by conventional diffraction methods. Recently, Hansen et al. revisited this electrochemical Li deintercalation from Li_xFeS_2 employing *in operando* XRD, *ex-situ* XANES and EXAFS analyses.[48] Their high-quality data confirmed that Li deintercalation oxidized both Fe^{2+} and S^{2-}, but the FeS_4 tetrahedra remained undistorted, confirming the suggestions from 1980s Mössbauer and EXAFS studies.[46] Also from the theoretical side, Wang et al. carried out computational structure prediction[49] using the evolutionary algorithm USPEX.[84] They found the series of structures in FeS_2 compositional space including Pyrite, Marcasite and the new metastable structure with *C*2/*m* space group (Figure 11a).

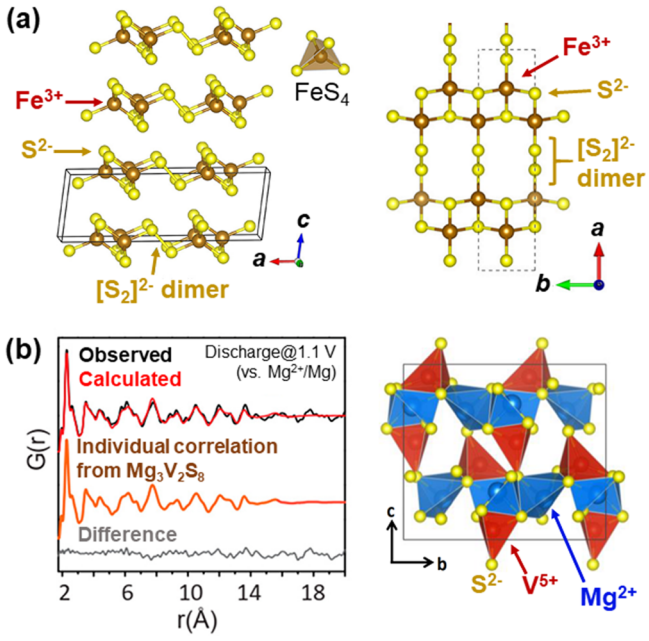

Figure 11. Uses of computational structure prediction for structure characterizations. (a) The structure of $Fe^{3+}S^{2-}[[S_2]^{2-}]_{1/2}$ (i.e., metastable FeS_2) predicted by the evolutionary algorithm USPEX. See Figure 3 for its electrochemical behavior. (b) X-ray pair distribution function data after electrochemical Mg intercalation into VS_4 using the USPEX-predicted $Mg_3V_2S_8$ structure. The right panel shows the structure after refinement. See also Figure 4b. Reprinted from refs 49 and 52. Copyright (2020) American Chemical Society.

This 2D vdW structure was composed of 1D $[Fe_2S_4]$ ribbons made of edge-sharing FeS_4 tetrahedra and bridged by S−S bonds. Its calculated band structure confirmed high-spin Fe^{3+} cations in tetrahedral coordination, coexisting with $[S_2]^{2-}$ and S^{2-} species. This observation was also consistent with early experimental studies.[45,46]

Obviously, those computational structure predictions become extremely useful when they are combined with local probe techniques. One good example was characterization of $Mg_3V_2S_8$ prepared by Mg intercalation into VS_4 (Figure 4b).[52] Although the chemical nature of $Mg_3V_2S_8$ could be well characterized by their ^{51}V NMR, XPS, and XANES analyses, its XRD did not show any diffraction arising from this Mg-intercalated phase. The hypothetical structure model was first acquired using USPEX, which was then subject to refinement against the pair distribution function data (PDF; see Figure 11b). The USPEX-predicted structure showed good agreement with the experimental X-ray pattern and revealed its structural evolution during electrochemical cycling.

Besides those generic crystallinity issues, stacking disorder has been a long-standing challenge in the structure characterization of intercalation compounds. 2D vdW systems and intercalation compounds (Figure 1a) often exhibit irregular stacking sequences. This causes severe *hkl*-dependent broadening of diffraction peaks, which must be modeled using large multilayered supercells.[104,105] In that sense, "zipper"-type architecture of polychalcogenides (Figure 1b) seems less susceptible to such stacking disorder, owing to their 3D networks interconnected by covalent anion−anion bonds. Contrary to such expectation, severe *hkl*-dependent peak broadening was observed also in the XRD of $Sr_2MnO_2Ch_2$ (Figure 12c), a layered polychalcogenide "zipped up" by multistep Cu deintercalation (see Figure 6). Stacking in layered polychalcogenides has a certain extent of flexibility arising from an orientational degree of freedom of chalcogen dimers (Figure 12a). For example, $[S_2]^{2-}$ dimers in $La_2O_2S_2$ completely lie in the its basal plane while those in $Ba_2F_2S_2$ tilt from the stacking axis by $\theta \sim 38°$, causing a different stacking sequence of the host PbO-type layers. Additionally, those $[S_2]^{2-}$ dimers may be subject to in-plane axial rotation by, e.g., $\varphi = \pm 90°$, which does not change local environment around the dimer, but introduce irregularity in their periodic stacking sequences (see ref 68 for the case study in $La_2O_2S_2$).

The XRD pattern in Figure 12c can be understood as an extreme case of such a stacking disorder of layered polychalcogenides. HAADF-STEM of the $Sr_2MnO_2Ch_2$ sample evidenced an irregular stacking sequence of their perovskite-type slabs, most likely arising from various orientation of chalcogen dimers.[74] In addition, ^7Li NMR revealed that residual Li/Cu intercalants also formed stacking faults. This complex stacking disorder was modeled by a large supercell approach in which one hundred $Sr_2MnO_2Ch_2$ layers were allowed to move individually relative to one another during the refinement (Figure 12b). This free-parameter approach similar to the one reported by Metz et al.[106] has successfully identified the most frequent stacking vectors (S_x, S_y) in their disordered stacking (Figure 12d). Such characterizations of stacking vectors provide ideas about possible local structures of disordered low-dimensional polychalcogenides. This conjectures may be further corroborated by other local probe analyses and computational structure predictions, ultimately enabling identifications of detailed structure models.

CONCLUSION

This Perspective presents a brief overview of anionic redox topochemistry as a tool to design novel solid-state materials. The basic concept of anionic redox topochemistry was established more than 30 years ago,[34,40,41] and several polychalcogenides have been examined as host frameworks.[45,55,56] These seminal studies were followed by extensive investigations aiming at secondary battery applications because anionic redox can be a promising way to boost energy density

https://doi.org/10.1021/acsorginorgau.3c00043
ACS Org. Inorg. Au 2024, 4, 26−40

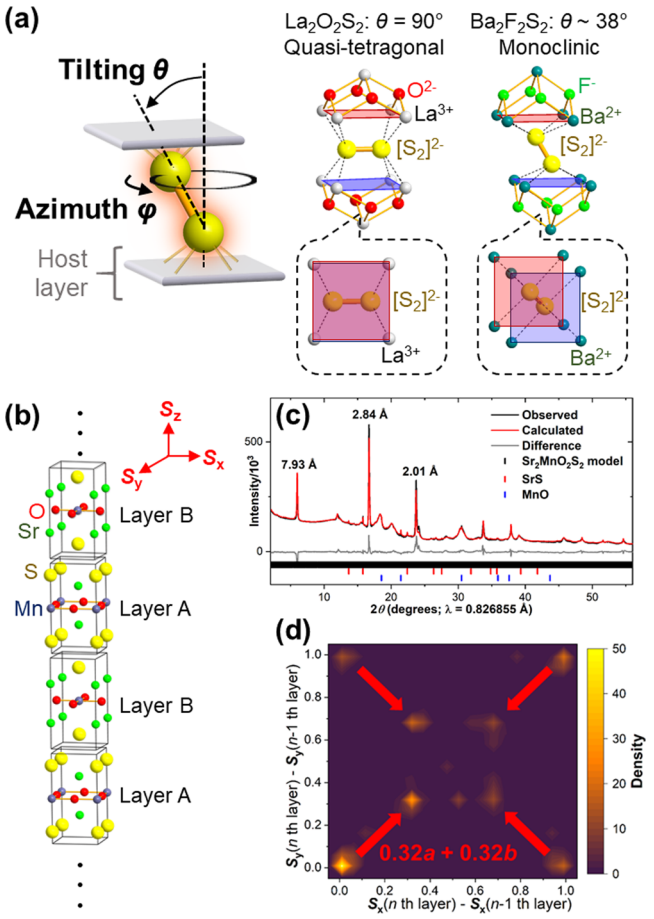

Figure 12. (a) Rotational degree of freedom of $[Ch_2]^{2-}$ dimers and its effects on stacking of host cationic layers in the cases of $La_2O_2S_2$ and $Ba_2F_2S_2$. (b) A hundred-layer supercell used for modeling disordered stacking in $Sr_2MnO_2Ch_2$ (see Figure 6) and (c) its Rietveld fit against the synchrotron XRD pattern. (d) 2D histogram showing refined in-plane stacking vectors (S_x, S_y) at respective layers relative to adjacent ones. Panels (b)−(d) were reprinted with permission under a Creative Commons Attribution 4.0 from ref 74. Copyright (2023) Springer Nature.

of cathode materials.[36,42−44] On the other hand, unique structure transformations involving anion−anion bond cleavages or formations have never been elucidated until a surge of such studies in the last 5 years.[26−28,50−52,70,71,74] This is in stark contrast to cationic redox topochemistry, where its structural chemistry and its uses to design novel electronic or magnetic materials[7] were examined in parallel with its application to secondary batteries.[13] This absence of materials design by anionic redox topochemistry can be ascribed to poor crystallinity of the products and its complex reaction manifolds where intercalation, conversion, and many other nontopochemical processes compete with each other. Recent advancements in syntheses and characterizations are resolving these issues.

Despite its challenging nature, anionic redox topochemistry enables unique types of structure transformations. One such process highlighted in this Perspective was "zipper"-type topochemistry (Figure 1b). Both processes, i.e., in situ 2D layer construction and topochemical conversion, clearly highlight the promise of anionic redox topochemistry. Now the next challenge will be to design functional materials with, e.g., promising electronic, magnetic, optical, and catalytic properties. As exemplified throughout the Perspective, such materials design will be achieved most likely through close collaborations between diverse experts across synthetic and computational chemistry, crystallography, spectroscopy, and condensed matter physics.

■ ASSOCIATED CONTENT

Data Availability Statement

The data underlying this study are available in the published article.

■ AUTHOR INFORMATION

Corresponding Author

Shunsuke Sasaki − *Nantes Université, CNRS, Institut des Matériaux de Nantes Jean Rouxel, IMN, F-44000 Nantes, France;* orcid.org/0000-0001-8358-1629; Email: Shunsuke.Sasaki@cnrs-imn.fr

Authors

Simon J. Clarke − *Department of Chemistry, University of Oxford, Inorganic Chemistry Laboratory, Oxford OX1 3QR, U.K.;* orcid.org/0000-0003-4599-8874

Stéphane Jobic − *Nantes Université, CNRS, Institut des Matériaux de Nantes Jean Rouxel, IMN, F-44000 Nantes, France;* orcid.org/0000-0002-1900-0030

Laurent Cario − *Nantes Université, CNRS, Institut des Matériaux de Nantes Jean Rouxel, IMN, F-44000 Nantes, France;* orcid.org/0000-0001-5720-4395

Complete contact information is available at: https://pubs.acs.org/10.1021/acsorginorgau.3c00043

Author Contributions

CRediT statement: **Shunsuke Sasaki** conceptualization, writing-original draft, writing-review and editing; **Stéphane Jobic** writing-review and editing; **Laurent Cario** writing-review and editing; **Simon J. Clarke** writing-review and editing.

Notes

The authors declare no competing financial interest.

■ ACKNOWLEDGMENTS

The authors acknowledge the financial support for the "Core-to-Core" collaborative project from CNRS IRP grant (Mixed Anions) and UK EPSRC grants (EP/T027991/1). S.S. thanks French National Research Agency for its financial support (ANR-23-CE08-0003) as well as JSPS Overseas Research Fellowship for the support during 2018-2020.

■ ABBREVIATIONS

vdW, van der Waals; HAADF-STEM, High-angle annular dark-field scanning transmission electron microscopy; XANES, X-ray absorption near-edge structure; XPS, X-ray photoelectron spectroscopy; USPEX, Universal Structure Predictor: Evolutionary Xtallography

■ REFERENCES

(1) Hille, F.; Richter, H.; Wong, S. P.; Bratovic, M.; Ressel, S.; Charpentier, E. The Biology of CRISPR-Cas: Backward and Forward. *Cell* **2018**, *172*, 1239−1259.

(2) Ruiz-Castillo, P.; Buchwald, S. L. Applications of Palladium-Catalyzed C−N Cross-Coupling Reactions. *Chem. Rev.* **2016**, *116*, 12564−12649.

(3) Rüdorff, W.; Hofmann, U. Über Graphitsalze. *Z. Anorg. Allg. Chem.* **1938**, *238*, 1−50.
(4) Lerf, A. Storylines in Intercalation Chemistry. *Dalton Trans.* **2014**, *43*, 10276−10291.
(5) Hofmann, U.; Endell, J. O. Die Abhängigkeit des Kationenaustausches und der Quellung bei Montmorillonit von der Vorerhitzung (Auszug). *Angew. Chem.* **1939**, *52*, 708−709.
(6) Rüdorff, W.; Sick, H. H. Einlagerungsverbindungen von Alkali- und Erdalkalimetallen in Molybdän- und Wolframdisulfid. *Angew. Chem.* **1959**, *71*, 127.
(7) Whittingham, M. S. Chemistry of Intercalation Compounds: Metal Guests in Chalcogenide Hosts. *Prog. Solid St. Chem.* **1978**, *12*, 41−99.
(8) Schöllhorn, R.; Kuhlmann, R.; Besenhard, J. O. Topotactic redox reactions and ion exchange of layered MoO_3 bronzes. *Mater. Res. Bull.* **1976**, *11*, 83−90.
(9) Delmas, C.; Cognac-Auradou, H.; Cocciantelli, J. M.; Ménétrier, M.; Doumerc, J. P. The $Li_xV_2O_5$ system: An overview of the structure modifications induced by the lithium intercalation. *Solid State Ionics* **1994**, *69*, 257−264.
(10) Coleman, C. C.; Goldwhite, H.; Tikkanen, W. A Review of Intercalation in Heavy Metal Iodides. *Chem. Mater.* **1998**, *10*, 2794−2800.
(11) Palvadeau, P.; Coic, L.; Rouxel, J.; Portier, J. The lithium and molecular intercalates of FeOCl. *Mater. Res. Bull.* **1978**, *13*, 221−227.
(12) Brec, R.; Schleich, D. M.; Ouvrard, G.; Louisy, A.; Rouxel, J. Physical properties of lithium intercalation compounds of the layered transition-metal chalcogenophosphites. *Inorg. Chem.* **1979**, *18*, 1814−1818.
(13) Whittingham, M. S. The Role of Ternary Phases in Cathode Reactions. *J. Electrochem. Soc.* **1976**, *123*, 315−320.
(14) Kriener, M.; Segawa, K.; Ren, Z.; Sasaki, S.; Wada, S.; Kuwabata, S.; Ando, Y. Electrochemical synthesis and superconducting phase diagram of $Cu_xBi_2Se_3$. *Phys. Rev. B* **2011**, *84*, No. 054513.
(15) Zhang, H.; Rousuli, A.; Zhang, K.; et al. Tailored Ising superconductivity in intercalated bulk $NbSe_2$. *Nat. Phys.* **2022**, *18*, 1425−1430.
(16) Borg, C. K. H.; Zhou, X.; Eckberg, C.; Campbell, D. J.; Saha, S. R.; Paglione, J.; Rodriguez, E. E. Strong anisotropy in nearly ideal tetrahedral superconducting FeS single crystals. *Phys. Rev. B* **2016**, *93*, No. 094522.
(17) Zhou, X.; Rodriguez, E. E. Tetrahedral Transition Metal Chalcogenides as Functional Inorganic Materials. *Chem. Mater.* **2017**, *29*, 5737−5752.
(18) Zhou, X.; Wilfong, B.; Vivanco, H.; Paglione, J.; Brown, C. M.; Rodriguez, E. E. Metastable layered cobalt chalcogenides from topochemical deintercalation. *J. Am. Chem. Soc.* **2016**, *138*, 16432−16442.
(19) Hayward, M. A.; Green, M. A.; Rosseinsky, M. J.; Sloan, J. Sodium Hydride as a Powerful Reducing Agent for Topotactic Oxide Deintercalation: Synthesis and Characterization of the Nickel(I) Oxide $LaNiO_2$. *J. Am. Chem. Soc.* **1999**, *121*, 8843−8854.
(20) Tsujimoto, Y.; Tassel, C.; Hayashi, N.; Watanabe, T.; Kageyama, H.; Yoshimura, K.; Takano, M.; Ceretti, M.; Ritter, C.; Paulus, W. Infinite-Layer Iron Oxide with a Square-Planar Coordination. *Nature* **2007**, *450*, 1062−1065.
(21) Li, D.; Lee, K.; Wang, B. Y.; Osada, M.; Crossley, S.; Lee, H. R.; Cui, Y.; Hikita, Y.; Hwang, H. Y. Superconductivity in an infinite-layer nickelate. *Nature* **2019**, *572*, 624−627.
(22) Kim, W. J.; Smeaton, M. A.; Jia, C.; Goodge, B. H.; Cho, B.-G.; Lee, K.; Osada, M.; Jost, D.; Levlev, A. V.; Moritz, B.; Kourkoutis, L. F.; Devereaux, T. P.; Hwang, H. Y. Geometric frustration of Jahn−Teller order in the infinite-layer lattice. *Nature* **2023**, *615*, 237−243.
(23) Fumagalli, G.; Stanton, S.; Bower, J. F. Recent Methodologies That Exploit C−C Single-Bond Cleavage of Strained Ring Systems by Transition Metal Complexes. *Chem. Rev.* **2017**, *117*, 9404−9432.
(24) Qin, Y.; Zhu, L.; Luo, S. Organocatalysis in Inert C−H Bond Functionalization. *Chem. Rev.* **2017**, *117*, 9433−9520.
(25) Clarke, J. B.; Hastie, J. W.; Kihlborg, L. H. E.; Metselaar, R.; Thackeray, M. M. Definitions of terms relating to phase transitions of the solid state (IUPAC Recommendations 1994). *Pure Appl. Chem.* **1994**, *66*, 577.
(26) Sasaki, S.; Driss, D.; Grange, E.; Mevellec, J.-Y.; Caldes, M. T.; Guillot-Deudon, C.; Cadars, S.; Corraze, B.; Janod, E.; Jobic, S.; Cario, L. A Topochemical Approach to Synthesize Layered Materials Based on the Redox Reactivity of Anionic Chalcogen Dimers. *Angew. Chem., Int. Ed.* **2018**, *57*, 13618−13623.
(27) Bhaskar, G.; Gvozdetskyi, V.; Batuk, M.; Wiaderek, K. M.; Sun, Y.; Wang, R.; Zhang, C.; Carnahan, S. L.; Wu, X.; Ribeiro, R. A.; Bud'ko, S. L.; Canfield, P. C.; Huang, W.; Rossini, A. J.; Wang, C.-Z.; Ho, K.-M.; Hadermann, J.; Zaikina, J. V. Topochemical Deintercalation of Li from Layered LiNiB: toward 2D MBene. *J. Am. Chem. Soc.* **2021**, *143*, 4213−4223.
(28) Sasaki, S.; Caldes, M. T.; Guillot-Deudon, C.; Braems, I.; Steciuk, G.; Palatinus, L.; Gautron, E.; Frapper, G.; Janod, E.; Corraze, B.; Jobic, S.; Cario, L. Design of Metastable Oxychalcogenide Phases by Topochemical (de)Intercalation of Sulfur in $La_2O_2S_2$. *Nat. Commun.* **2021**, *12*, No. 3605.
(29) Poizot, P.; Laruelle, S.; Grugeon, S.; Dupont, L.; Tarascon, J.-M. Nano-sized transition-metal oxides as negative-electrode materials for lithium-ion batteries. *Nature* **2000**, *407*, 496−499.
(30) Shao-Horn, Y.; Osmialowski, S.; Horn, Q. C. Reinvestigation of Lithium Reaction Mechanism is FeS_2 Pyrite at Ambient Temperature. *J. Electrochem. Soc.* **2002**, *149*, A1547−A1555.
(31) Butala, M. M.; Mayo, M.; Doan-Nguyen, V. V. T.; Lumley, M. A.; Göbel, C.; Wiaderek, K. M.; Borkiewicz, O. J.; Chapman, K. W.; Chupas, P. J.; Balasubramanian, M.; Laurita, G.; Britto, S.; Morris, A. J.; Grey, C. P.; Seshadri, R. Local Structure Evolution and Modes of Charge Storage in Secondary Li−FeS_2 Cells. *Chem. Mater.* **2017**, *29*, 3070−3082.
(32) Zou, J.; Zhao, J.; Wang, B.; Chen, S.; Chen, P.; Ran, Q.; Li, L.; Wang, X.; Yao, J.; Li, H.; Huang, J.; Niu, X.; Wang, L. Unraveling the Reaction Mechanism of FeS_2 as a Li-Ion Battery Cathode. *ACS Appl. Mater. Interfaces* **2020**, *12*, 44850−44857.
(33) Soulard, C.; Rocquefelte, X.; Petit, P.-E.; Evain, M.; Jobic, S.; Itié, J.-P.; Munsch, P.; Koo, H.-J.; Whangbo, M.-H. Experimental and Theoretical Investigation on the Relative Stability of the PdS_2- and Pyrite-Type Structures of $PdSe_2$. *Inorg. Chem.* **2004**, *43*, 1943−1949.
(34) Jobic, S.; Brec, R.; Rouxel, J. Occurrence and Characterization of Anionic Bondings in Transition Metal Dichalcogenides. *J. Alloys Compd.* **1992**, *178*, 253−283.
(35) Manzeli, S.; Ovchinnikov, D.; Pasquier, D.; Yazyev, O. V.; Kis, A. 2D transition metal dichalcogenides. *Nat. Rev. Mater.* **2017**, *2*, No. 17033.
(36) Goodenough, J. B.; Kim, Y. Locating redox couples in the layered sulfides with application to $Cu[Cr_2]S_4$. *J. Solid State Chem.* **2009**, *182*, 2904−2911.
(37) Yokoyama, M.; Yoshimura, M.; Wakihara, M.; Somiya, S.; Taniguchi, M. Synthesis of vanadium sulfides under high pressure. *J. Solid State Chem.* **1985**, *60*, 182−187.
(38) Murphy, D. W.; Cros, C.; Di Salvo, F. J.; Waszczak, J. V. Preparation and Properties of Li_xVS_2 ($0 < x < 1$). *Inorg. Chem.* **1977**, *16*, 3027−3031.
(39) DiSalvo, F. J.; Eibschutz, M.; Cros, C.; Murphy, D. W.; Waszczak, J. V. Magnetic and Mössbauer studies of $Li_xM_yV_{1-y}S_2$ (M = Fe or Cr). *Phys. Rev. B* **1979**, *19*, 3441−3448.
(40) Rouxel, J. Anion- Cation Redox Competition and the Formation of New Compounds in Highly Covalent Systems. *Chem.—Eur. J.* **1996**, *2*, 1053−1059.
(41) Schöllhorn, R. From Electronic/Ionic Conductors to Superconductors: Control of Materials Properties. *Angew. Chem., Int. Ed.* **1988**, *27*, 1392−1400.
(42) Saha, S.; Assat, G.; Sougrati, M. T.; Foix, D.; Li, H.; Vergnet, J.; Turi, S.; Ha, Y.; Yang, W.; Cabana, J.; Rousse, G.; Abakumov, A. M.; Tarascon, J.-M. Exploring the Bottlenecks of Anionic Redox in Li-rich Layered Sulfides. *Nat. Energy* **2019**, *4*, 977−987.

https://doi.org/10.1021/acsorginorgau.3c00043
ACS Org. Inorg. Au 2024, 4, 26−40

(43) Lu, Z.; Dahn, J. R. Understanding the Anomalous Capacity of $Li/Li[Ni_xLi_{(1/3-2x/3)}Mn_{(2/3-x/3)}]O_2$ Cells Using In Situ X-Ray Diffraction and Electrochemical Studies. *J. Electrochem. Soc.* **2002**, *149*, A815−A822.
(44) Assat, G.; Tarascon, J.-M. Fundamental understanding and practical challenges of anionic redox activity in Li-ion batteries. *Nat. Energy* **2018**, *3*, 373−386.
(45) Dugast, A.; Brec, R.; Ouvrard, G.; Rouxel, J. Li_2FeS_2, a Cathodic Material for Lithium Secondary Battery. *Solid State Ionics* **1981**, *5*, 375−378.
(46) Brec, R.; Prouzet, E.; Ouvrard, G. Redox Processes in the Li_xFeS_2/Li Electrochemical System Studied through Crystal, Mössbauer, and EXAFS Analyses. *J. Power Sources* **1989**, *26*, 325−332.
(47) Gard, P.; Sourisseau, C.; Ouvrard, G.; Brec, R. Infrared Study of Lithium Intercalated Phases in the $LixFeS_2$ System ($0 \leq x \leq 2$). Characterization of a New Iron Disulfide. *Solid State Ionics* **1986**, *20*, 231−238.
(48) Hansen, C. J.; Zak, J. J.; Martinolich, A. J.; Ko, J. S.; Bashian, N. H.; Kaboudvand, F.; der Ven, A.; Melot, B. C.; Nelson Weker, J.; See, K. A. Multielectron, Cation and Anion Redox in Lithium-Rich Iron Sulfide Cathodes. *J. Am. Chem. Soc.* **2020**, *142*, 6737−6749.
(49) Wang, B.; Braems, I.; Sasaki, S.; Guégan, F.; Cario, L.; Jobic, S.; Frapper, G. Prediction of a New Layered Polymorph of FeS_2 with $Fe^{3+}S^{2-}(S_2^{2-})_{1/2}$ Structure. *J. Phys. Chem. Lett.* **2020**, *11*, 8861−8866.
(50) Elgaml, M.; Cassidy, S. J.; Clarke, S. J. Topochemical intercalation reactions of $ZrSe_3$. *J. Solid State Chem.* **2022**, *314*, No. 123436.
(51) Fujioka, M.; Jeem, M.; Sato, K.; Tanaka, M.; Morita, K.; Shibuya, T.; Takahashi, K.; Iwasaki, S.; Miura, A.; Nagao, M.; Demura, S.; Sakata, H.; Ono, M.; Kaiju, H.; Nishii, J. Intercalation on Transition Metal Trichalcogenides via a Quasi-Amorphous Phase with 1D Order. *Adv. Funct. Mater.* **2023**, *33*, No. 2208702.
(52) Dey, S.; Lee, J.; Britto, S.; Stratford, J. M.; Keyzer, E. N.; Dunstan, M. T.; Cibin, G.; Cassidy, S. J.; Elgaml, M.; Grey, C. P. Exploring Cation−Anion Redox Processes in One-Dimensional Linear Chain Vanadium Tetrasulfide Rechargeable Magnesium Ion Cathodes. *J. Am. Chem. Soc.* **2020**, *142*, 19588−19601.
(53) Island, J. O.; Molina-Mendoza, A. J.; Barawi, M.; Biele, R.; Flores, E.; Clamagirand, J. M.; Ares, J. R.; van der Zant, H. S. J.; D'Agosta, R.; Ferrer, I. J.; Castellanos-Gomez, A. Electronics and optoelectronics of quasi-1D layered transition metal trichalcogenides. *2D Mater.* **2017**, *4*, No. 022003.
(54) Conejeros, S.; Guster, B.; Alemany, P.; Pouget, J.-P.; Canadell, E. Rich Polymorphism of Layered NbS_3. *Chem. Mater.* **2021**, *33*, 5449−5463.
(55) Chianelli, R. R.; Dines, M. B. Reaction of *n*-Butyllithium with Transition Metal Trichalcogenides. *Inorg. Chem.* **1975**, *14*, 2417−2421.
(56) Murphy, D.; Trumbore, F. A. The Chemistry of TiS_3 and $NbSe_3$ Cathodes. *J. Electrochem. Soc.* **1976**, *123*, 960−964.
(57) Powell, A. V. Chapter 7. Intercalation compounds of low-dimensional transition metal chalcogenides. *Annu. Rep. Prog. Chem., Sect. C: Phys. Chem.* **1993**, *90*, 177−213.
(58) Sourisseau, C.; Gwet, S. P.; Gard, P.; Mathey, Y. Structural, optical, and electronic properties of Li_3MS_3 compounds (M^{III} = Ti, Zr, Hf). *J. Solid State Chem.* **1988**, *72*, 257−271.
(59) Canadell, E.; Thieffry, C.; Mathey, Y.; Whangbo, M.-H. Energy Factors Governing the Partial Irreversibility of Lithium Intercalation in Layered Trichalcogenides MX_3 (M = Ti, Zr, Hf; X = S, Se) and the Structural Changes in the Intercalated Species Li_3MX_3. *Inorg. Chem.* **1989**, *28*, 3043−3047.
(60) Trumbore, F. A. Niobium triselenide: A unique rechargeable positive electrode material. *J. Power Sources* **1989**, *26*, 65−75.
(61) Luo, L.; Zhao, B.; Xiang, B.; Wang, C.-M. Size-Controlled Intercalation-to-Conversion Transition in Lithiation of Transition-Metal Chalcogenides—$NbSe_3$. *ACS Nano* **2016**, *10*, 1249−1255.
(62) Allmann, R.; Baumann, I.; Kutoglu, A.; Rosch, H.; Hellner, E. Die Kristallstruktur des Patronits $V(S_2)_2$. *Naturwissenschaften.* **1964**, *51*, 263−264.
(63) Rout, C. S.; Kim, B.-H.; Xu, X.; Yang, J.; Jeong, H. Y.; Odkhuu, D.; Park, N.; Cho, J.; Shin, H. S. Synthesis and Characterization of Patronite Form of Vanadium Sulfide on Graphitic Layer. *J. Am. Chem. Soc.* **2013**, *135*, 8720−8725.
(64) Wang, Y.; Liu, Z.; Wang, C.; Yi, X.; Chen, R.; Ma, L.; Hu, Y.; Zhu, G.; Chen, T.; Tie, Z.; Ma, J.; Jin, Z. Highly Branched VS_4 Nanodendrites with 1D Atomic-Chain Structure as a Promising Cathode Material for Long-Cycling Magnesium Batteries. *Adv. Mater.* **2018**, *30*, No. 1802563.
(65) Britto, S.; Leskes, M.; Hua, X.; Hébert, C.-A.; Shin, H. S.; Clarke, S.; Borkiewicz, O.; Chapman, K. W.; Seshadri, R.; Cho, J.; Grey, C. P. Multiple Redox Modes in the Reversible Lithiation of HighCapacity, Peierls-Distorted Vanadium Sulfide. *J. Am. Chem. Soc.* **2015**, *137*, 8499−8508.
(66) Li, Z.; Vinayan, B. P.; Jankowski, P.; Njel, C.; Roy, A.; Vegge, T.; Maibach, J.; Lastra, J. M. G.; Fichtner, M.; Zhao-Karger, Z. Multi-Electron Reactions Enabled by Anion-Based Redox Chemistry for High-Energy Multivalent Rechargeable Batteries. *Angew. Chem., Int. Ed.* **2020**, *59*, 11483−11490.
(67) Driss, D.; Cadars, S.; Deniard, P.; Mavellec, J.-Y.; Corraze, B.; Janod, E.; Cario, L. Crystal structure and chemical bonding in the mixed anion compound BaSF. *Dalton Trans.* **2017**, *46*, 16244−16250.
(68) Mvélé, L.-B.; Sasaki, S.; Latouche, C.; Deniard, P.; Janod, E.; Braems, I.; Jobic, S.; Cario, L. Revisiting the Crystal Structure of Layered Oxychalcogenides $Ln_2O_2S_2$ (Ln = La, Pr, and Nd). *Inorg. Chem.* **2023**, *62*, 7264−7272.
(69) Sasaki, S.; Steciuk, G.; Guillot-Deudon, C.; Caldes, M. T.; Isabelle, B.; Janod, E.; Corraze, B.; Jobic, S.; Cario, L. Solvothermal and mechanochemical intercalation of Cu into $La_2O_2S_2$ enabled by the redox reactivity of $(S_2)^{2-}$ pairs. *Dalton Trans.* **2021**, *50*, 12419−12423.
(70) Sasaki, S.; Lesault, M.; Grange, E.; Janod, E.; Corraze, B.; Cadars, S.; Caldes, M. T.; Guillot-Deudon, C.; Jobic, S.; Cario, L. Unexplored reactivity of $(S_n)^{2-}$ oligomers with transition metals in low-temperature solid-state reactions. *Chem. Commun.* **2019**, *55*, 6189−6192.
(71) Chaupatnaik, A.; Abakumov, A. M.; Rousse, G.; Foix, D.; Louis, J.; Leube, B. T.; Tarascon, J.-M. Electrochemical Exploration of Layered Cu-Based Oxychalcogenides Obtained Topochemically via Anionic Redox and Displacement Reaction. *Chem. Mater.* **2023**, *35*, 5924−5935.
(72) Cassidy, S. J.; Pitcher, M. J.; Lim, J. J. K.; Hadermann, J.; Allen, J. P.; Watson, G. W.; Britto, S.; Chong, E. J.; Free, D. G.; Grey, C. P.; Clarke, S. J. Layered CeSO and LiCeSO Oxide Chalcogenides Obtained via Topotactic Oxidative and Reductive Transformations. *Inorg. Chem.* **2019**, *58*, 3838−3850.
(73) Blandy, J. N.; Abakumov, A. M.; Christensen, K. E.; Hadermann, J.; Adamson, P.; Cassidy, S. J.; Ramos, S.; Free, D. G.; Cohen, H.; Woodruff, D. N.; Thompson, A. L.; Clarke, S. J. Soft Chemical Control of the Crystal and Magnetic Structure of a Layered Mixed Valent Manganite Oxide Sulfide. *APL Mater.* **2015**, *3*, No. 041520.
(74) Sasaki, S.; Giri, S.; Cassidy, S. J.; Dey, S.; Batuk, M.; Vandemeulebroucke, D.; Cibin, G.; Smith, R. I.; Holdship, P.; Grey, C. P.; Hadermann, J.; Clarke, S. J. Anion redox as a means to derive layered manganese oxychalcogenides with exotic intergrowth structures. *Nat. Commun.* **2023**, *14*, No. 2917.
(75) Gál, Z. A.; Rutt, O. J.; Smura, C. F.; Overton, T. P.; Barrier, N.; Clarke, S. J.; Hadermann, J. Structural Chemistry and Metamagnetism of an Homologous Series of Layered Manganese Oxysulfides. *J. Am. Chem. Soc.* **2006**, *128*, 8530−8540.
(76) Dey, S.; Zeng, D.; Adamson, P.; Cabana, J.; Indris, S.; Lu, J.; Clarke, S. J.; Grey, C. P. Structural Evolution of Layered Manganese Oxysulfides during Reversible Electrochemical Lithium Insertion and Copper Extrusion. *Chem. Mater.* **2021**, *33*, 3989−4005.
(77) Santos-Cottin, D.; Casula, M.; Lantz, G.; Klein, Y.; Petaccia, L.; Le Févre, P.; Bertran, F.; Papalazarou, E.; Marci, M.; Gauzzi, A. Rashba Coupling Amplification by a Staggered Crystal Field. *Nat. Commun.* **2016**, *7*, No. 11258.

https://doi.org/10.1021/acsorginorgau.3c00043
ACS Org. Inorg. Au 2024, 4, 26−40

(78) Takahashi, H.; Sugimoto, A.; Nambu, Y.; Yamauchi, T.; Hirata, Y.; Kawakami, T.; Avdeev, M.; Matsubayashi, K.; Du, F.; Kawashima, C.; Soeda, H.; Nakano, S.; Uwatoko, Y.; Ueda, Y.; Sato, T. J.; Ohgushi, K. Pressure-induced superconductivity in the iron-based ladder material $BaFe_2S_3$. *Nat. Mater.* **2015**, *14*, 1008−1012.
(79) Thackeray, M. M.; Kang, S.-H.; Johnson, C. S.; Vaughey, J. T.; Benedeka, R.; Hackney, S. A. Li_2MnO_3-stabilized $LiMO_2$ (M = Mn, Ni, Co) electrodes for lithium-ion batteries. *J. Mater. Chem.* **2007**, *17*, 3112−3125.
(80) McCalla, E.; Abakumov, A. M.; Saubanère, M.; Foix, D.; Berg, E. J.; Rousse, G.; Doublet, M.-L.; Gonbeau, D.; Novák, P.; Van Tendeloo, G.; Dominko, R.; Tarascon, J.-M. Visualization of O-O peroxo-like dimers in high-capacity layered oxides for Li-ion batteries. *Science* **2015**, *350*, 1516−1521.
(81) Pearce, P.; Perez, A.; Rousse, G.; Saubanère, M.; Batuk, D.; Foix, D.; McCalla, E.; Abakumov, A. M.; Van Tendeloo, G.; Doublet, M.-L.; Tarascon, J.-M. Evidence for anionic redox activity in a tridimensional-ordered Li-rich positive electrode β-Li_2IrO_3. *Nat. Mater.* **2017**, *16*, 580−586.
(82) Böttcher, P.; Doert, Th.; Arnold, H.; Tamazyan, R. Contribution to the crystal chemistry of rare earth chalcogenides. I. The compounds with layer structures LnX_2. *Z. Kristallogr.* **2000**, *215*, 246−253.
(83) Larquet, C.; Carenco, S. Metal Oxysulfides: From Bulk Compounds to Nanomaterials. *Front. Chem.* **2020**, *8*, No. 179.
(84) Oganov, A. R.; Lyakhov, A. O.; Valle, M. How evolutionary crystal structure prediction works − and why. *Acc. Chem. Res.* **2011**, *44*, 227−237.
(85) Mvélé, L.-B.; Sasaki, S.; Deniard, P.; Tsujimoto, Y.; Janod, E.; Guillot-Deudon, C.; Caldes, M. T.; Braems, I.; Corraze, B.; Jobic, S.; Cario, L. Synthesis of Non-centrosymmetric, Metastable Rare-Earth Oxysulfides by Anionic Redox Topochemistry. *Chem. Mater.* **2023**, *35*, 7597−7604.
(86) Friedrich, D.; Schlosser, M.; Näther, C.; Pfitzner, A. In Situ X-ray Diffraction Study of the Thermal Decomposition of Selenogallates $Cs_2[Ga_2(Se_2)_{2-x}Se_{2+x}]$ (x = 0, 1, 2). *Inorg. Chem.* **2018**, *57*, 5292−5298.
(87) Friedrich, D.; Schlosser, M.; Pfitzner, A. Interconversion of One-Dimensional Thiogallates $Cs_2[Ga_2(S_2)_{2-x}S_{2+x}]$ (x = 0, 1, 2) by Using High-Temperature Decomposition and Polysulfide-Flux Reactions. *Cryst. Growth Des.* **2017**, *17*, 4887−4892.
(88) Seel, F. Sulfur in Artwork: Lapis Lazuli and Ultramarine Pigments. *Stud. Inorg. Chem.* **1984**, *5*, 67−89.
(89) Warner, T. E.; Andersen, J. H. The effects of sulfur intercalation on the optical properties of artificial 'hackmanite', $Na_8[Al_6Si_6O_{24}]$-$Cl_{1.8}S_{0.1}$; 'sulfosodalite', $Na_8[Al_6Si_6O_{24}]S$; and natural tugtupite, $Na_8[Be_2Al_2Si_8O_{24}](Cl,S)_{2-\delta}$. *Phys. Chem. Minerals* **2012**, *39*, 163−168.
(90) Gobeltz-Hautecoeur, N.; Demortier, A.; Lede, B.; Lelieur, J. P.; Duhayon, C. Occupancy of the Sodalite Cages in the Blue Ultramarine Pigments. *Inorg. Chem.* **2002**, *41*, 2848−2854.
(91) Yurlov, I. S.; Ushakova, Y. N.; Medvedeva, O. V.; Kalinina, L. A.; Shirokova, G. I.; Ananchenko, B. A. Determination of Diffusion Coefficients for Sulfide Ions in Solid Electrolytes on the Basis of $BaSm_2S_4$ and $CaGd_2S_4$. *Russ. J. Electrochem.* **2007**, *43*, 638−643.
(92) Ananchenko, B. A.; Koshurnikova, E. V.; Kalinina, L. A.; Ushakova, Y. N.; Bezdenezhnykh, L. A. Transport Properties of Sulfide-Conductive Solid Electrolyte in the System $CaYb_2S_4$−Yb_2S_3. *Glass Phys. Chem.* **2012**, *38*, 402−412.
(93) Lei, T.; Gu, M.; Fu, H.; Wang, J.; Wang, L.; Zhou, J.; Liu, H.; Lu, B. Bond modulation of $MoSe_{2+x}$ driving combined intercalation and conversion reactions for high performance K cathodes. *Chem. Sci.* **2023**, *14*, 2528−2536.
(94) De Souza, R. A. Oxygen Diffusion in $SrTiO_3$ and Related Perovskite Oxides. *Adv. Funct. Mater.* **2015**, *25*, 6326−6342.
(95) Cario, L.; Sasaki, S.; Jobic, S.; Caldes, M. T.; Janod, E.; Corraze, B.; Braems, I.; Mvele, L.-B.; Deudon, C. G. Electrochemical Cells Based on Intercalation and Deintercalation of Chalcogen Anions. PCT Int. WO2022136707A1, June 30, 2022.
(96) Nowroozi, M. A.; Mohammad, I.; Molaiyan, P.; Wissel, K.; Munnangi, A. R.; Clemens, O. Fluoride ion batteries − past, present, and future. *J. Mater. Chem. A* **2021**, *9*, 5980−6012.
(97) Fujioka, M.; Wu, C.; Kubo, N.; Zhao, G.; Inoishi, A.; Okada, S.; Demura, S.; Sakata, H.; Ishimaru, M.; Kaiju, H.; Nishii, J. Proton-Driven Intercalation and Ion Substitution Utilizing Solid-State Electrochemical Reaction. *J. Am. Chem. Soc.* **2017**, *139*, 17987−17993.
(98) Halasz, I. Single-Crystal-to-Single-Crystal Reactivity: Gray, Rather than Black or White. *Cryst. Growth Des.* **2010**, *10*, 2817−2823.
(99) Yajima, T.; Takeiri, F.; Aidzu, K.; Akamatsu, H.; Fujita, K.; Yoshimune, W.; Ohkura, M.; Lei, S.; Gopalan, V.; Tanaka, K.; Brown, C. M.; Green, M. A.; Yamamoto, T.; Kobayashi, Y.; Kageyama, H. A labile hydride strategy for the synthesis of heavily nitridized $BaTiO_3$. *Nat. Chem.* **2015**, *7*, 1017−1023.
(100) Li, H.-B.; Kobayashi, S.; Zhong, C.; Namba, M.; Cao, Y.; Kato, D.; Kotani, Y.; Lin, Q.; Wu, M.; Wang, W.-H.; Kobayashi, M.; Fujita, K.; Tassel, C.; Terashima, T.; Kuwabara, A.; Kobayashi, Y.; Takatsu, H.; Kageyama, H. Dehydration of Electrochemically Protonated Oxide: $SrCoO_2$ with Square Spin Tubes. *J. Am. Chem. Soc.* **2021**, *143*, 17517−17525.
(101) Martinolich, A. J.; Neilson, J. R. Toward Reaction-by-Design: Achieving Kinetic Control of Solid State Chemistry with Metathesis. *Chem. Mater.* **2017**, *29*, 479−489.
(102) Zhang, S.; Yoshikawa, M.; Inumaru, K.; Yamanaka, S. Topochemical Cross-Linking of the $[Hf_2N_2]$ Layers with Sulfur in α-HfNBr. *Inorg. Chem.* **2013**, *52*, 10571−10575.
(103) Kamysbayev, V.; Filatov, A. S.; Hu, H.; Rui, X.; Lagunas, F.; Wang, D.; Klie, R. F.; Talapin, D. V. Covalent surface modifications and superconductivity of two-dimensional metal carbide MXenes. *Science* **2020**, *369*, 979−983.
(104) Casas-Cabanas, M.; Reynaud, M.; Rikarte, J.; Horbach, P.; Rodríguez-Carvajal, J. FAULTS: a program for refinement of structureswith extended defects. *J. Appl. Crystallogr.* **2016**, *49*, 2259−2269.
(105) Mangelsen, S.; Srinivasan, B. R.; Schürmann, U.; Kienle, L.; Näther, C.; Bensch, W. Nanostructured tungsten sulfides: insights into precursor decomposition and the microstructure using X-ray scattering methods. *Dalton Trans.* **2019**, *48*, 1184−1201.
(106) Metz, P.; Koch, R.; Cladek, B.; Page, K.; Neuefeind, J.; Misture, S. X-ray and neutron total scattering analysis of H_y·$(Bi_{0.2}Ca_{0.55}Sr_{0.25})(Ag_{0.25}Na_{0.75})Nb_3O_{10}$·$xH_2O$ perovskite nanosheet booklets with stacking disorder. *Powder Diffr.* **2016**, *31*, 126−134.

https://doi.org/10.1021/acsorginorgau.3c00043
ACS Org. Inorg. Au 2024, 4, 26−40